Review | Open Access

Energy Materials

Xu *et al. Energy Mater.* **2026**, *6*, 600140 **DOI:**10.20517/energymater.2026.238

Metal-organic framework/MXene composites: design strategies and applications for energy storage, catalysis, and sensing

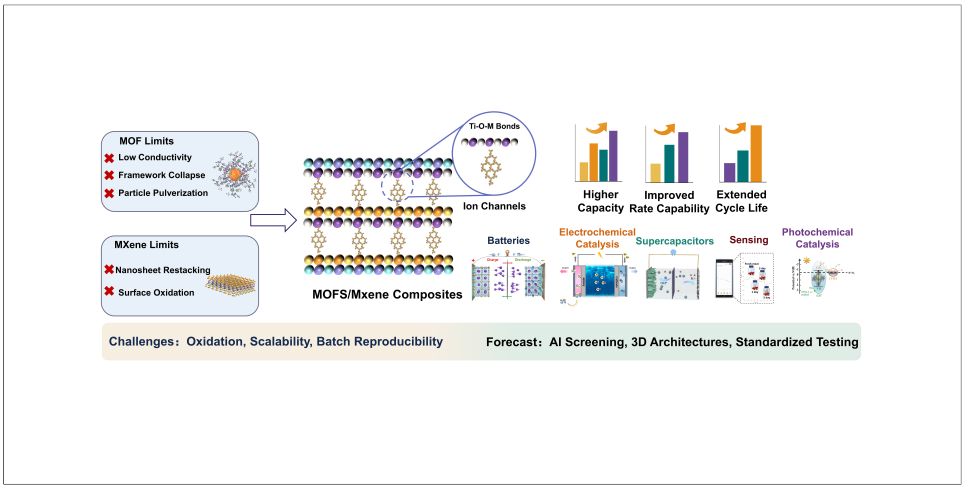
Ben Xu[1,2,*], Mingxu Sun[1,2], Ziyi Li[1,2], Ji Ma[1,2], Fei Zhao[1,2], Xinyu Wang[1,2], Daofeng Sun[1,2,*]

Keywords:
MOF/MXene composites, electrocatalysis, energy storage and conversion, photocatalysis, interfacial design, advanced functional materials

Citation: Xu, B.; Sun, M.; Li, Z.; Ma, J.; Zhao, F.; Wang, X.; Sun, D. Metal-organic framework/MXene composites: design strategies and applications for energy storage, catalysis, and sensing. *Energy Mater.* **2026**, *6*, 600140. https://dx.doi.org/10.20517/energymater.2026.238

Received: 24 Jul 2026
First Decision: 20 Aug 2026
Revised: 16 Sep 2026
Accepted: 23 Sep 2026
Published: 22 Oct 2026

Academic Editor:
Ho Seok Park
Copy Editor:
Fangling Lan
Production Editor:
Fangling Lan



Abstract

Metal-organic frameworks (MOFs), as crystalline porous materials with tunable chemical compositions, have attracted widespread interest for energy-related applications. However, their low electrical conductivity and limited structural stability under electrochemical conditions restrict practical deployment. Integrating MOFs with two-dimensional transition metal carbides/nitrides (MXenes) creates composite materials that combine the high surface area and active sites of MOFs with the metallic conductivity and mechanical flexibility of MXenes. This review summarizes recent progress on MOF/MXene composites. The major synthetic routes are classified into four categories: *in situ* growth with interfacial chemical bonding, electrostatic self-assembly, post-synthetic transformation into metal oxides, sulfides, and phosphides, and interface engineering. Their applications are discussed across electrochemical energy storage (lithium, sodium, potassium, and zinc-ion batteries, and supercapacitors), energy conversion (electrocatalytic hydrogen/oxygen evolution, oxygen reduction, and photocatalysis), and sensing. Despite research advances, challenges remain for practical application, including MXene oxidation during processing and operation, difficulties in large-scale fabrication

Check for updates

[1]School of Materials Science and Engineering, China University of Petroleum (East China), Qingdao 266580, Shandong, China.
[2]Key Laboratory of Heavy Oil, China University of Petroleum (East China), Qingdao 266580, Shandong, China.

***Correspondence to:** Dr. Ben Xu, Dr. Daofeng Sun, School of Materials Science and Engineering, China University of Petroleum (East China), Qingdao 266580, Shandong, China; Key Laboratory of Heavy Oil, China University of Petroleum (East China), Qingdao 266580, Shandong, China. E-mail: benxu@upc.edu.cn; dfsun@upc.edu.cn

with batch-to-batch consistency, and the need for precise interfacial regulation. Finally, future research directions are outlined, including artificial intelligence-assisted material screening, construction of three-dimensional hierarchical structures, and evaluation of industrial applicability through standardized testing protocols.

INTRODUCTION

Growing fossil fuel consumption and environmental degradation have intensified global interest in sustainable energy storage and conversion technologies. Rechargeable batteries, supercapacitors, and electrocatalysts for water splitting and fuel cells are critical components for utilizing renewable energy. The development of advanced electrode materials with high energy density, adequate power density, extended cycle life, and acceptable rate performance remains essential for advancing these technologies. Metal-organic frameworks (MOFs) have emerged as a class of functional materials characterized by regular porous frameworks, high specific surface areas (often exceeding 1,000 $m^2 g^{-1}$), and flexible structural modulation[1-3]. MOFs are assembled through coordination bonds between metal ions or secondary building units and organic linkers, forming periodic networks with controllable pore geometry and chemical functionality[4-6]. The modular synthesis of MOFs enables the rational design of redox-active metal centers (Co, Ni, Fe, Cu, Mn, *etc.*) and incorporation of functional organic groups, making them inherently suitable for electrochemical applications[7-10]. Typical examples include zeolitic imidazolate frameworks (ZIFs) such as ZIF-67 and ZIF-8, which exhibit thermal stability and nitrogen-rich composition[10,11], as well as carboxylate-based MOFs (e.g., HKUST-1, MOF-5) and materials institute lavoisier (MIL)-series materials with diverse metal coordination environments. These structural features facilitate ion transport and electrolyte penetration, rendering MOFs promising candidates for supercapacitor electrodes, battery active materials, and electrocatalysts[12].

Nevertheless, pristine MOFs exhibit inherent limitations that constrain their practical use in electrochemical systems. First, their electrical conductivity typically ranges from 10^{-8} to 10^{-5} S m^{-1}. This low conductivity arises from localized electronic states of metal nodes and insulating organic linkers, which impedes electron transport, increases internal resistance, and degrades rate and power performance[13-15]. Second, many MOFs are structurally unstable during long-term electrochemical cycling. Repeated ion insertion/extraction and redox reactions may weaken the coordination bonds between metal nodes and organic ligands, leading to framework collapse, particle pulverization, and capacity decay[16,17]. In addition, the high porosity of MOFs results in relatively low volumetric energy density, and large volume variations during cycling can further accelerate structural damage and weaken contact between active materials and current collectors.

To address these limitations, researchers have developed multiple strategies to improve the electrochemical performance of MOF-based materials. One approach involves the synthesis of conductive MOFs, in which conjugated linkers or mixed-valence metal centers form delocalized electron pathways that enhance intrinsic conductivity[18]. Another approach is high-temperature pyrolysis or carbonization of MOFs under inert or reductive atmospheres, converting MOFs into porous carbon composites embedded with metal nanoparticles, metal oxides, or metal chalcogenides. Such derivatives retain the porous architecture of the original MOFs while gaining higher conductivity and structural robustness[19,20]. However, high-temperature processing usually reduces the crystallinity and specific surface area of MOFs, decreasing the number of available active sites. Furthermore, the batch-to-batch reproducibility of pyrolyzed MOFs remains a concern due to sensitivity to temperature gradients and atmosphere control.

Hybridizing MOFs with conductive substrates represents an alternative strategy that combines the merits of different components through composite design. Graphene, carbon nanotubes (CNTs), and conductive polymers have been widely adopted as supporting materials to improve the conductivity and mechanical

strength of MOF electrodes[8,21,22]. Recently, two-dimensional (2D) transition metal carbides, nitrides, and carbonitrides, collectively named MXenes, have emerged as substrates for MOF modification. MXenes offer distinct advantages over traditional carbon materials, including higher metallic conductivity, hydrophilic surfaces, and tunable terminal chemistry[3,9,12].

MXenes follow the general formula $M_{n+1}X_nT_x$, where M refers to early transition metals (Ti, Mo, Nb, V), X stands for carbon and/or nitrogen, and T_x represents surface terminal groups (-O, -OH, -F)[23-26]. First reported in 2011 by selective etching of Al layers from MAX phases, typical MXenes including $Ti_3C_2T_x$, Ti_2NT_x, $Mo_2TiC_2T_x$, and Nb_2CT_x exhibit metallic conductivity comparable to or higher than multilayered graphene. For instance, single-layer $Ti_3C_2T_x$ reaches approximately 8,000 S cm^{-1}[27]. It is important to note that the reported electrical conductivity values of MXenes vary widely across the literature, ranging from 2,000 to 10,000 S cm^{-1}, depending on the specific synthesis conditions, delamination methods, and flake sizes[28-31]. They also feature hydrophilic surfaces and mechanical flexibility[32]. The terminal groups introduced during etching enable MXenes to disperse in aqueous and organic solutions, facilitating solution-based processing. Moreover, the negatively charged surface and functional groups of MXenes can serve as nucleation sites for MOF crystal growth, enabling interfacial interaction and uniform distribution of active phases[33-37].

The combination of MOFs and MXenes forms heterostructures that offset the weaknesses of individual materials. MXene nanosheets serve as conductive skeletons to build electron transport channels, prevent MOF particle aggregation, and buffer structural strain during electrochemical cycling[38]. Their metallic nature ensures electron transfer to redox-active MOF centers and compensates for the poor conductivity of pure MOFs. In turn, MOF particles or their derivatives act as spacers to suppress the restacking of MXene nanosheets, a common issue that reduces the available surface area and blocks ion diffusion in pristine MXene electrodes. Meanwhile, the porous MOF structure provides active sites for electrochemical reactions, relieves volume expansion in batteries, and contributes pseudocapacitance in supercapacitors. Chemical bonds such as Ti-O-Co, Ti-O-Ni, and Ti-O-Zn can form at the MOF/MXene interface, which may rearrange local electron density and influence reaction kinetics[13,32,39]. The resulting composites integrate the electric double-layer capacitance of MXenes and the surface redox pseudocapacitance of MOFs, with improved structural stability and reaction dynamics. MOF/MXene composites can be constructed into diverse architectures, including 0D/2D, 1D/2D, 2D/2D, and 3D hierarchical structures, allowing targeted optimization of ion/electron transport and mechanical properties for different applications[40,41].

From a mechanistic perspective, the performance gains arise from several mutually reinforcing effects rather than from conductivity enhancement alone. First, interfacial charge redistribution at the MOF/MXene junction—mediated by coordination bonds such as Ti-O-Co, Ti-O-Ni, Ti-N, and Zr-O—is proposed to lower the charge-transfer resistance and tune the adsorption energetics of reaction intermediates (H*, OH*, Li^+, Na^+, Zn^{2+}), providing a plausible electronic origin of the improved rate capability and catalytic activity[19,32,33,42,43]. Second, the flexible MXene network mechanically confines alloy- and conversion-type active materials, buffering the large volume changes and suppressing pulverization[17,44,45]. Third, intercalated MOF layers act as nanospacers that prevent MXene restacking and keep ion-transport channels open[15]. Fourth, the two components stabilize each other, although the protection of the MXene is only partial—environmental TEM and molecular-dynamics studies show that hydrofluoric acid (HF)-etched $Ti_3C_2T_x$ oxidizes even at room temperature, and oxidation stability remains the central durability bottleneck[46,47].

Owing to these synergistic effects, MOF/MXene composites have demonstrated performance improvements in various energy-related fields. In lithium-ion, sodium-ion, potassium-ion, and zinc-ion rechargeable batteries, the conductive network and structural buffering effect enhance specific capacity, rate capability,

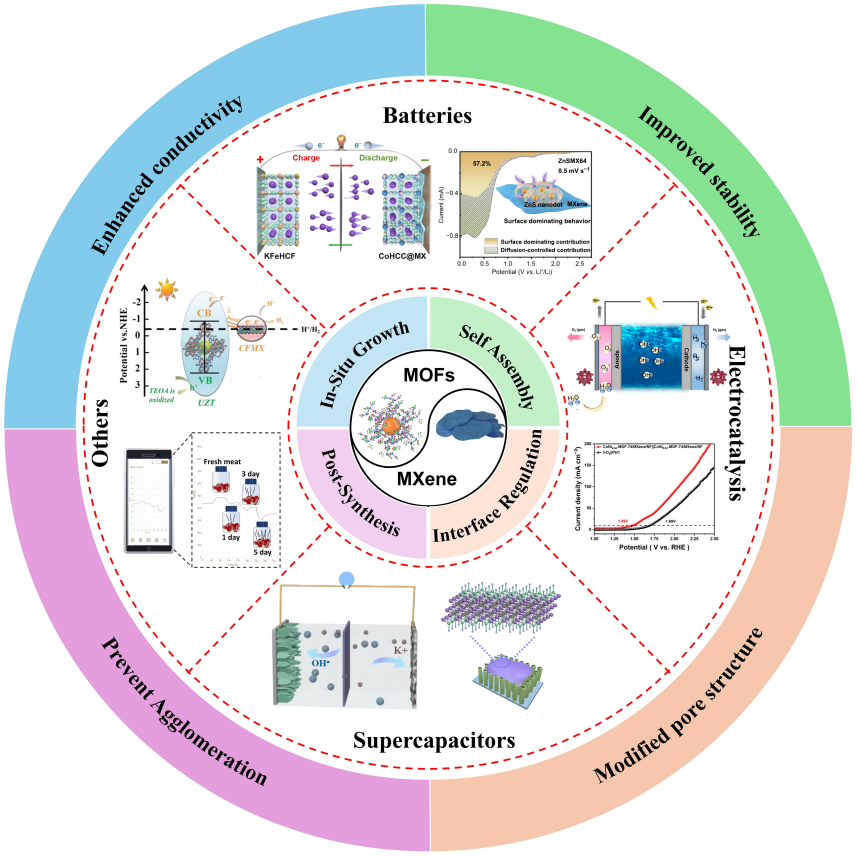


Figure 1. Strategies and applications of MOF/MXene composites. Batteries: adapted from Ref.[62,63], under CC BY 4.0 license. Electrocatalysis: adapted from Ref.[64], under CC BY 4.0 license. Supercapacitors: adapted from Ref.[65], under CC BY 4.0 license. Others (sensing and photocatalysis): adapted from Ref.[66,61], under CC BY 4.0 license.

and cycling stability[48-50]. For supercapacitors, the coexistence of electric double-layer capacitance and pseudocapacitance contributes to energy and power density, while the flexibility of MXenes supports the fabrication of wearable energy storage devices[51-56]. In electrocatalysis, maximized exposed active sites and accelerated charge transfer enable these heterostructures to function as catalysts for hydrogen evolution reaction (HER), oxygen evolution reaction (OER), and oxygen reduction reaction (ORR)[19,57,58]. They also show potential in photocatalysis[59-61]. The synthetic strategies and application scope of MOF/MXene composites are summarized in Figure 1.

Although several reviews have surveyed MOF/MXene hybrids, the present work complements rather than duplicates them. Venkateswarlu *et al.* organized the field by dimensionality and confined their discussion to electrochemical storage and the HER, OER, and ORR, with coverage ending in 2023[1]. Cao *et al.* later extended the scope to radionuclide and heavy metal capture, microwave attenuation, and gas separation, but treated zinc-based batteries and sensing only briefly[2]. Three distinctions characterize this review. First, a pristine versus derived taxonomy is applied throughout, which proves essential for the OER, where the MOF acts as a sacrificial precursor to the working metal oxyhydroxide phase on MXene (Section "Electrochemical catalysis"). Second, representative test conditions are tabulated, and metric inflating practices and industrial benchmarks are critically assessed (Sections "Batteries" to "Photochemical catalysis"). Third, coverage is broadened across zinc ion, the nitrogen reduction (NRR), methanol oxidation (MOR), and CO_2 reduction (CO_2RR), room temperature and wearable sensing, and photocatalytic H_2, CO_2, and N_2 conversion with quantum efficiency analysis (Sections "Sensing applications" and "Photochemical catalysis"). This scope,

taxonomy, and critical perspective position the review as an application-oriented complement to existing surveys[1,2].

This review focuses on synthetic strategies for MOF/MXene heterostructures, including *in situ* growth with interfacial bonding, electrostatic self-assembly, post-synthetic derivation, and interface engineering. Meanwhile, we analyze structure-performance relationships based on recent literature, evaluate their performance in energy storage and conversion systems, as well as in sensing and photocatalysis, and discuss current limitations in large-scale production, long-term stability, and reproducibility. Finally, we propose future research directions, covering AI-assisted material design, advanced structural engineering, and the industrial translation of laboratory achievements.

STRATEGIES OF MOF/MXene COMPOSITING

Synthetic methods determine the interfacial contact state, distribution of active phases, and overall electrochemical performance of MOF/MXene composites. To realize synergistic effects rather than simple physical mixing, it is essential to coordinate MOF crystallization behavior with MXene surface chemistry. In this review, fabrication approaches are classified into four categories: *in situ* growth with chemical bonding, electrostatic self-assembly, post-synthetic derivation, and interface engineering. Each strategy creates distinct structural and interfacial features, which affect charge transport, mechanical stability, and electrochemical activity. The selection of a specific strategy depends on the target application, the chemical stability of the MOF precursor, and the terminal group composition of the MXene.

In situ growth through chemical bonding

In situ growth is a widely used method to prepare MOF/MXene composites. In this route, MOF crystals nucleate and grow directly on MXene surfaces via coordination or covalent interactions. This method can achieve tight interfacial contact, maximize charge transfer area, and avoid phase separation caused by physical mixing. MXenes possess abundant -O, -OH, and -F terminal groups derived from etching processes. These hydrophilic groups improve dispersion in polar solvents and can anchor metal ions through electrostatic attraction and coordination bonds[67-69].

The formation of interfacial chemical bonds during *in situ* growth is considered important for electron transport between insulating MOFs and conductive MXenes. For example, Co^{2+} and Ni^{2+} ions can coordinate with oxygen-containing groups on $Ti_3C_2T_x$ to form Ti-O-Co or Ti-O-Ni bridges, which may act as electron conduction pathways[32,33]. These bridging bonds are proposed to reduce charge-transfer resistance and influence redox reaction kinetics. Yang *et al.* found that low-temperature annealing at 300 °C could regulate the content of Ti-O-Co bonds in Co-BDC/$Ti_3C_2T_x$ composites. Optimized interfacial coupling improved electron transfer and enhanced supercapacitor performance[32]. However, the exact correlation between bond density and electrochemical performance remains incompletely quantified, and the long-term stability of these interfacial bonds under electrochemical polarization requires further investigation.

Solvothermal and hydrothermal methods are commonly adopted to control the size, morphology, and distribution of *in situ* grown MOFs. MXene nanosheets serve as heterogeneous nucleation sites to form dispersed MOF nanoparticles or nanosheets instead of large aggregated crystals[70-73] [Figure 2A]. For instance, bimetallic Ni/Co-MOF nanosheets grown on MXene via solvothermal treatment show uniform coverage and adhesion, and remain stable during electrochemical cycling[74]. Similarly, Co^{2+} can coordinate with 2-methylimidazole on $Ti_3C_2T_x$ surfaces to anchor ZIF-67 polyhedrons. The obtained hierarchical structures combine the pseudocapacitance of MOFs and the conductivity of MXenes[15,71]. Nevertheless, hydrothermal conditions can also promote MXene oxidation, particularly when the etching-derived terminal

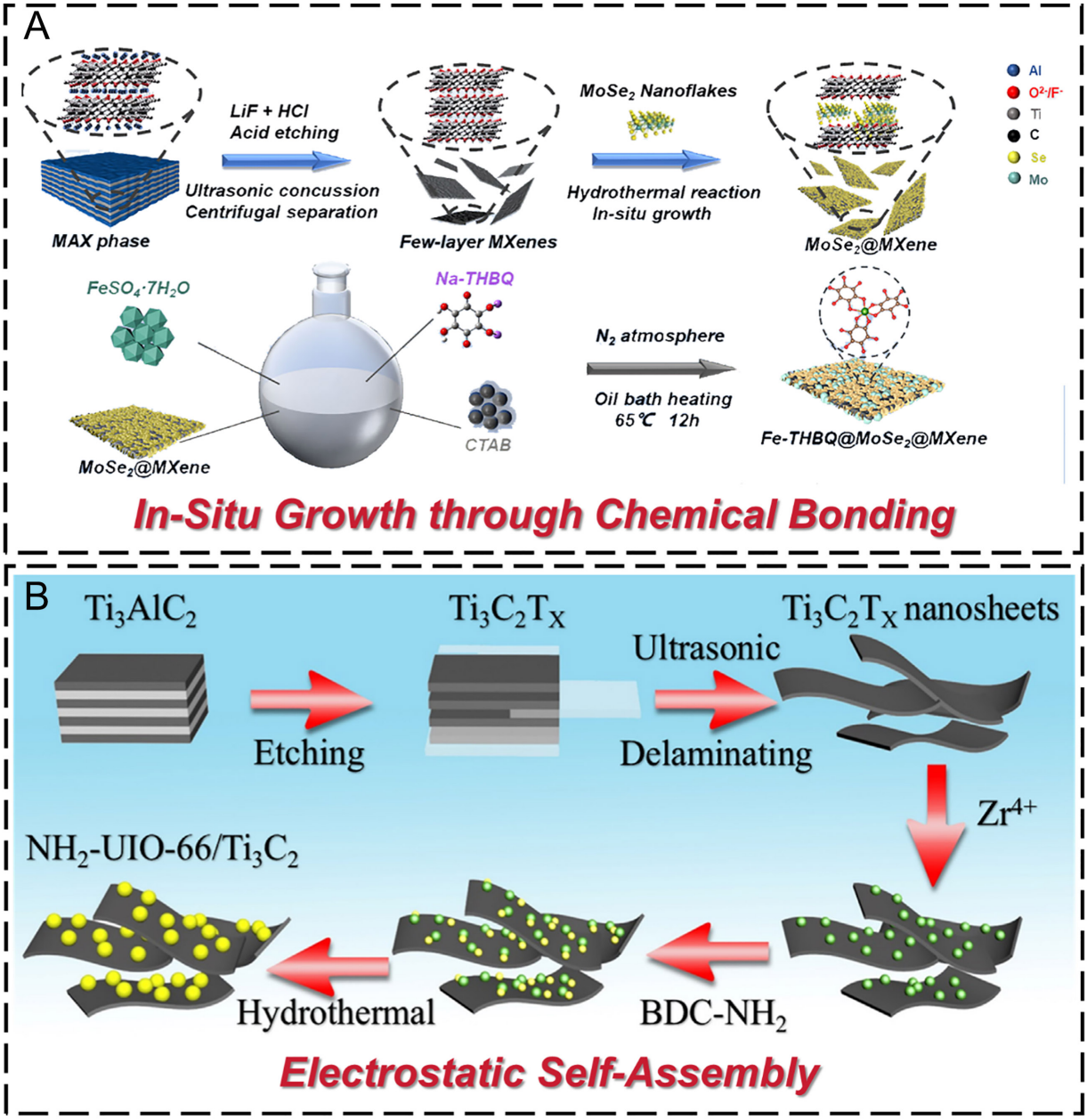


Figure 2. (A) *In situ* growth of Fe-THBQ@$MoSe_2$@MXene composite via interfacial Fe-Se coordination. Adapted from Ref.[70], under CC BY 4.0 license. (B) Electrostatic self-assembly of Zr-MOF/MXene composite. Adapted from Ref.[75], under CC BY 4.0 license.

groups are predominantly -F, which may hydrolyze under solvothermal conditions and compromise the conductivity of the MXene substrate.

In situ growth also enables the fabrication of 2D/2D heterostructures, in which ultrathin MOF nanosheets align on MXene basal planes. This structure can enlarge the exposed active area and shorten ion diffusion paths. Xiao *et al.* synthesized 2D/2D $Ti_3C_2T_x$/NiCo MOF heterostructures, in which carboxyl groups on MOF linkers bonded with MXene terminal groups[14]. The interface maintained structural integrity during lithium-ion battery cycling. The matched dimensions of the two components optimize electrochemical interfaces and provide mechanical strength. However, the uniform synthesis of ultrathin MOF nanosheets remains challenging, and the control of MOF layer thickness on MXene surfaces is often empirical rather than predictive.

The *in situ* growth method offers direct interfacial bonding, but its applicability depends on the compatibility between MOF synthesis conditions and MXene stability. MOFs synthesized under strongly acidic or basic conditions may degrade MXene nanosheets, and the formation of dense MOF coatings can block the ion-accessible surface of MXenes[46,47,75]. Therefore, reaction parameters such as pH, temperature, and solvent polarity must be carefully optimized for each MOF/MXene pair.

Electrostatic self-assembly

Different from *in situ* growth, which relies on chemical reactions, electrostatic self-assembly constructs MOF/MXene heterostructures through physical interactions between oppositely charged materials. MXene nanosheets carry negative zeta potential in aqueous and organic dispersions due to deprotonated -O^- and fluorine terminals, so they can assemble with positively charged MOF particles and derivatives[77-79]. This method is suitable for combining pre-synthesized MOFs with specific morphologies and for building complex multilayer structures that are difficult to obtain via direct growth.

Layer-by-layer electrostatic assembly is an effective way to prepare 2D/2D heterostructures, and has been used, for example, to couple pre-formed Zr-MOF nanosheets with MXene while preserving their crystallinity[75] [Figure 2B]. Alternate deposition of MXene and MOF nanosheets forms ordered superlattices with intimate interfacial contact[40,80]. Such structures provide active sites and electron pathways, while preventing the restacking of 2D materials. As a typical case, ZIF-67-derived $CoNi_2S_4$ nanocubes can bind with few-layer $Ti_3C_2T_x$ via electrostatic interaction to form interconnected 3D networks, which facilitate ion and electron transport in supercapacitor electrodes[81]. Electrostatic interaction ensures distribution of active materials on MXene networks and can enhance rate capability and cycling stability. However, the strength of electrostatic forces is sensitive to electrolyte pH and ionic strength, which may limit the stability of assembled structures in some electrochemical environments.

Vacuum-assisted filtration is a scalable technique to convert electrostatically assembled dispersions into free-standing flexible films with controllable thickness and packing density[82]. During filtration, negatively charged MXene sheets and positively charged MOF particles stack alternately to form a "brick-and-mortar" structure, which combines the mechanical strength of MXenes and the electrochemical activity of MOFs. These flexible films can be directly used as electrodes without extra binders or conductive additives, increasing volumetric energy density and simplifying device fabrication. The mild conditions of electrostatic assembly preserve the crystallinity and porosity of both components and retain their intrinsic electrochemical properties. A limitation is that the mechanical stability of films under repeated bending or stretching depends on the interlayer adhesion strength, which is weaker than covalent bonding and may lead to delamination under mechanical stress.

Post-synthetic derivation

Post-synthetic strategies refer to the chemical or thermal transformation of prefabricated MOF/MXene hybrids into functional derivatives, including metal oxides, sulfides, phosphides, selenides, and nitrogen-doped carbon. Although pristine MOFs have high surface area and regular structures, their low conductivity and limited chemical stability under electrochemical conditions necessitate further modification. The MXene substrate provides mechanical support during transformation, inhibits nanoparticle aggregation, and maintains electrical connectivity throughout the composite[83,84].

Thermal annealing under controlled atmospheres is a typical post-synthetic treatment. For example, ZIF-67 grown on MXene can be carbonized under inert atmosphere to obtain Co nanoparticle-embedded nitrogen-doped carbon (Co/NC) supported on $Ti_3C_2T_x$. The composites integrate the catalytic activity of Co, the conductivity of MXenes, and the carbon matrix[85]. Phosphorization can convert MOF/MXene precursors

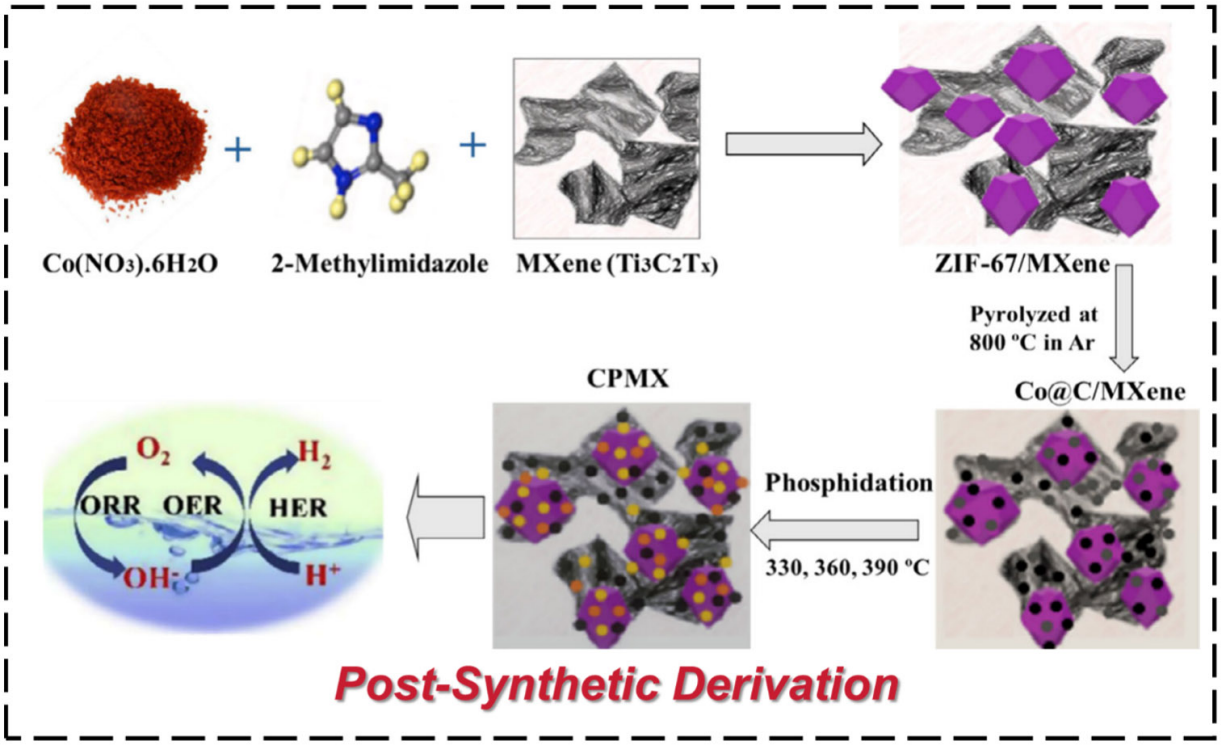


Figure 3. Post-synthetic derivation of CoP@C/$Ti_3C_2T_x$ composite. Adapted from Ref.[90], under CC BY 4.0 license.

into metal phosphides such as CoP and Ni_2P, which exhibit activity for hydrogen evolution and improved lithium storage capacity[86-90] [Figure 3]. The MXene skeleton maintains structural integrity during high-temperature treatment, prevents porous framework collapse, and maintains contact between active phases and conductive substrates. However, high-temperature processing often induces partial MXene oxidation, particularly for Ti-based MXenes, and the resulting TiO_2 surface layer can increase interfacial contact resistance. The balance between MOF carbonization efficiency and MXene preservation requires precise temperature control.

Sulfidation and selenation are also used to convert MOF/MXene precursors into metal chalcogenides with modified electrochemical performance. For example, thermal treatment of ZIF-67/$Ti_3C_2T_x$ hybrids with sulfur sources yields Co_9S_8/MXene and Ni_3S_4/CuS/MXene sandwich structures, which deliver higher specific capacity and rate performance for supercapacitors and batteries[83,91,92]. These derivatives usually have hierarchical porous structures to buffer volume expansion during ion insertion, while MXenes provide continuous electron pathways and mechanical reinforcement. It should be noted that the sulfidation process often requires sulfur vapor or thiourea at elevated temperatures, which may etch the MXene surface and alter its terminal group chemistry. In general, post-synthetic derivation bridges the gap between the high surface area of MOFs and the practical requirements for conductivity and stability in electrochemical devices, but the structural complexity of the final product makes it difficult to establish precise structure-performance correlations.

Interface engineering

Beyond conventional growth and assembly methods, interface engineering is developed to regulate the interaction between MOFs and MXenes, so as to optimize electronic structures and electrochemical kinetics. Surface modification of MXenes before MOF loading is an approach to improve interfacial compatibility and charge transfer efficiency. For example, ammonia annealing induces nitrogen doping on $Ti_3C_2T_x$, which

enlarges interlayer spacing and improves surface wettability[93,94]. These changes promote uniform MOF growth and enhance ion accessibility.

Introducing functional interlayers between MOFs and MXenes is another strategy to modulate interfacial properties. Singha *et al.* inserted ultrathin hexagonal boron nitride (h-BN) between ZIF-67-derived carbon and MXene to construct MOF-MXene-BN heterostructures[38]. The dielectric interlayer optimizes charge injection and avoids direct chemical reaction between MOF derivatives and MXenes, thus improving the cycling stability of supercapacitors. Similarly, amination treatment endows MXene surfaces with positive or neutral charges, which improves the wettability and adhesion of MOF coatings. This method has been applied to fabricate Ni/Co-MOF@TCT-NH_2 composites with enhanced electrochemical performance[74]. However, the addition of interlayers inevitably increases the overall internal resistance of the electrode and may reduce the volumetric energy density.

Other chemical functionalization methods include creating defects and vacancies on MXene surfaces to serve as MOF nucleation sites and pre-anchoring metal ions on MXene edges to guide oriented MOF crystallization. These refined engineering methods enable regulation of interfacial electronic states, induce charge redistribution, and can boost the intrinsic activity of catalytic sites[34,58]. Rational interface design can make MOF/MXene composites exceed the simple performance superposition of individual components and approach the theoretical limit of synergistic interaction. Nevertheless, many interface engineering strategies involve multi-step processing with low yields, which complicates scale-up. The long-term stability of engineered interfaces under continuous electrochemical operation remains insufficiently documented.

The role of interfacial bonding in charge transfer

Interfacial M-O-Ti bonds (M = Co, Ni, Zn, Zr) are frequently invoked to explain the faster charge transfer observed in MOF/MXene composites. The experimental basis for bond formation is comparatively strong. X-ray photoelectron spectroscopy (XPS) consistently reveals shifts in the Ti 2p, O 1s, and metal 2p binding energies that point to Ti-O-Co, Ti-O-Ni, Ti-N, and Zr-O coordination environments, as documented for Co-BDC/$Ti_3C_2T_x$ [32], NiCo hydroxide grown on MXene[13], and the 2D/2D CoBDC/$Ti_3C_2T_x$ heterostructure[33]. Density functional theory (DFT) calculations complement these observations by showing charge-density redistribution at MOF/MXene junctions and modified adsorption energetics of reaction intermediates such as H*, OH*, Li^+, Na^+, and Zn^{2+}[19,42,43,58]. Hierarchical electron-coupling engineering in F-doped NiFe layered double hydroxide (LDH)/MOF-74 grown on $Ti_3C_2T_x$ has been shown by combined XPS and DFT analysis to redistribute interfacial charge and optimize the adsorption of oxygen-containing intermediates, directly correlating interfacial coupling with enhanced overall water splitting[95]; NiCoP/$Ti_3C_2T_x$ interfaces were further calculated to lower the kinetic energy barrier of alkaline hydrogen evolution[96]. These electronic effects are accompanied by a measurable reduction in charge-transfer resistance relative to physical mixtures or bare MOFs[19,32,33].

At the same time, the causal weight assigned to interfacial bonds is less securely established. A quantitative relationship between bond density and electrochemical performance has not been demonstrated: most studies report one or a few annealing or growth conditions together with a performance optimum, without independently quantifying the number or density of M-O-Ti linkages. The frequently repeated claim that a higher density of M-O-Ti bonds accelerates electron transfer and thereby improves capacity or activity therefore remains a plausible hypothesis rather than an established mechanism. Even the XPS evidence requires caution, because peak deconvolution in the Ti 2p, C 1s, and O 1s regions of $Ti_3C_2T_x$ is prone to misassignment, and published spectra frequently disagree on component attribution[97]. These considerations indicate that interfacial M-O-Ti bonding is best regarded as a well-supported contributor to charge transfer whose quantitative structure-performance relationship and long-term stability under polarization remain open questions.

Table 1. Summary of the key advantages, main drawbacks, and typical applications of the four strategies

Strategy	Interfacial bonding	Key advantage	Main drawback	Typical application
In situ growth	Covalent/coordination (Ti-O-M, Ti-N)[13,32,33,98]	Strongest interface; uniform dispersion[14,32,71]	MXene oxidation in solvothermal step; batch-limited[46,47,75]	SC, LIBs, OER/HER[32,43,33,98]
Electrostatic self-assembly	Physical (electrostatic/H-bond)[76,80,81]	Mild; Preserves crystallinity; multilayer films[40,76,80]	Weak adhesion; pH/ionic-strength sensitive[35,81]	Films, Li-S, sensing[54,99,100]
Post-synthetic derivation	Mixed, partially preserved[84,89]	Highest conductivity/activity[16,78,89]	Loses MOF porosity; MXene oxidation; complex product[46,47,101]	SIB/PIB anodes, HER/OER, SC[16,45,89,92]
Interface engineering	Engineered bonds/interlayers[38,93,94]	Finest electronic tuning[95,96]	Multi-step; low yield; high cost[35,38]	Bifunctional catalysis, Zn anodes[42,95,102]

MOF: Metal-organic framework; LIBs: lithium-ion batteries; OER: oxygen evolution reaction; HER: hydrogen evolution reaction; SIB: sodium-ion battery; PIB: potassium-ion battery; SC: supercapacitors.

Taken together, the four strategies offer complementary trade-offs. *In situ* growth gives the strongest interfacial bonding and the most uniform MOF dispersion, but is sensitive to solvothermal conditions, risks MXene oxidation, and is batch-limited. Electrostatic self-assembly is mild and preserves the crystallinity of both components, yet yields weaker physical adhesion that is sensitive to electrolyte pH and ionic strength. Post-synthetic derivation raises intrinsic conductivity and activity most effectively, but sacrifices MOF crystallinity and porosity, risks MXene oxidation, and complicates identification of the true active phase. Interface engineering offers the finest electronic tuning and can exceed simple performance superposition, but is multi-step, low-yield, and costly. In practice the four routes are often combined to balance interfacial strength, activity, and manufacturability[35]. Table 1 summarizes the key advantages, main drawbacks, and typical applications of these strategies.

APPLICATIONS OF MOF/MXene COMPOSITES

Throughout this section, P denotes composites retaining the crystalline MOF framework and D denotes MOF-derived hybrids. As summarized in Tables 2 and 3, MOF/MXene heterostructures exhibit wide applications spanning electrochemical energy storage, electrocatalysis, sensing, and photochemical fields. The following sections discuss the design mechanisms and structural advantages underlying these applications.

Batteries

Before discussing individual battery types, several common design principles emerge from the literature. First, the conductive MXene network is indispensable for compensating the poor electronic conductivity of MOF-derived active materials, ensuring efficient charge transfer during redox reactions. Second, interfacial engineering, whether through chemical bonding between MXene surface terminations and MOF linkers or through heterojunction creation, plays a critical role in stabilizing electrode structures during volume changes accompanying ion insertion. Third, structural hierarchy spanning from nanoscale void spaces to microscale electrode configurations must be carefully orchestrated to accommodate ion size while maintaining mechanical integrity. These principles manifest differently across lithium, sodium, potassium, and zinc-based systems, as detailed below.

Lithium-ion batteries (LIBs)

The limited performance of conventional graphite anodes—theoretical capacity of 372 mAh g^{-1}, sluggish Li^+ redox kinetics, and irreversible structural degradation—remains a core bottleneck for LIB advancement.

Table 2. MOF/MXene composites for electrochemical energy storage and electrocatalysis

Material	Application	Performance	Test conditions	Ref.
Si/MXene@C (D)	Li-ion battery	1,006.1 mAh g^{-1}@100 mA g^{-1}, Si-O-Ti bonds	CR2025 half-cell; 1 M $LiPF_6$ EC/DEC (1:1); 0.01-3 V; 100 mA g^{-1}; 150 cycles; loading n.r.	[44]
nMOF-867/$Ti_3C_2T_x$ (P)	Li-S battery	1,302 mAh g^{-1}@0.2C, 624 mAh g^{-1} after 500 cycles	CR2025 half-cell; 1 M LiTFSI + 2 wt% $LiNO_3$ in DOL/DME (1:1); 1.7-2.8 V; 0.2C (1C = 1,672 mA g^{-1}); 500 cycles; loading 1.2 mg cm^{-2} (sulfur)	[98]
MXene@CoS_2/NC (D)	Na-ion battery	620 mAh g^{-1}@0.2 A g^{-1}, hollow structure	CR2032 half-cell; 1 M $NaCF_3SO_3$ in diglyme; 0.25-3.0 V; 0.2 A g^{-1}; 200 cycles; loading 1.2 mg cm^{-2}	[16]
ZnTe@C/$Ti_3C_2T_x$ (D)	K-ion battery	408 mAh g^{-1}@0.1 A g^{-1}, 230.2 mAh g^{-1}@1.0 A g^{-1} after 3,500 cycles, 0D/2D confinement	CR2032 half-cell; 4 M KFSI in DME; 0.01-3.0 V; 0.1 A g^{-1} (rate); 1.0 A g^{-1}; 3,500 cycles; loading 0.9 mg cm^{-2}	[45]
$Ti_3C_2O_2$/CuHHB (P)	Zn-ion battery (anode)	Dendrite-free plating,HER suppression	N/A (computational study)	[42]
Cu-HHTP/MXene (P)	Zn-ion battery (cathode)	260.1 mAh g^{-1}@0.1 A g^{-1}, 92.5%@1,000 cycles (4 A g^{-1})	Zn/Cu-HHTP/MX full cell; 2 M $Zn(CF_3SO_3)_2$; 0.5-1.3 V; 0.1 A g^{-1} (rate); 4.0 A g^{-1}; 1,000 cycles; loading 1.5 mg cm^{-2}	[99]
ZnCo-MnO/C/Ti_3C_2@Zn (D)	Zn-ion full cell	428.9 mAh g^{-1}@0.1 A g^{-1}, 98.7%@3,000 cycles (3.0 A g^{-1})	Full cell (ZnCo-MnO/C//Ti_3C_2@Zn); 2 M $ZnSO_4$ + 0.1 M $MnSO_4$; 0.8-1.9 V; 0.1 A g^{-1} (rate); 3.0 A g^{-1}; 3,000 cycles; loading 1.0-1.4 mg cm^{-2}	[100]
CoP/C@Nb_2CT_x (D)	HER/OER bifunctional	η_{10} = 50 mV (HER), 149 mV (OER)	Three-electrode; 0.1 M KOH; 1.1-1.8 V (OER)/-0.6-0 V (HER) *vs.* RHE; 5 mV s^{-1}; 2,000 CV cycles; loading n.r.	[89]
Fe-N-C@$Ti_3C_2T_x$ (D)	ORR (Fuel cells)	$E_{1/2}$ = 0.887 V (alkaline), 0.777 V (acidic)	RRDE three-electrode; 0.1 M KOH/0.1 M $HClO_4$; 0.065-1.065 V *vs.* RHE; 1,600 rpm; 10,000 CV cycles; loading 0.56 mg cm^{-2}	[19]
BTC-NiCoCuO/MXene (D)	Overall water splitting	1.38 V@10 mA cm^{-2} (bifunctional)	Two-electrode system; 1 M KOH; 0.2-2.2 V; 10 mA cm^{-2}; 24 h CP; loading n.r.	[101]
ZIF-67@Ti_3C_2 (P)	Nitrogen reduction (NRR)	6.52 μmol h^{-1} cm^{-2}, FE = 20.2%	Three-electrode system; 0.1 M KOH; -0.2 to -0.6 V *vs.* RHE; -0.4 V; 2 h chronoamperometry; loading n.r.	[102]
$NiCo_2S_4$@Co_3S_4/$Ti_3C_2T_x$ (D)	Asymmetric supercapacitor	1,872 F g^{-1}@2 mV s^{-1}, 92.2%@12,000 cycles, 241.9 Wh kg^{-1} (device)	Three-electrode system; 3 M KOH; -0.1-0.6 V; 2 mV s^{-1}; 10 A g^{-1}; 12,000 cycles; loading n.r.	[79]

P: Pristine MOF/MXene composite; D: MOF-derived/MXene hybrid; OER: oxygen evolution reaction; HER: hydrogen evolution reaction; ORR: oxygen reduction reaction; RHE: reversible hydrogen electrode.

Table 3. MOF/MXene composites for sensing and photochemical applications

Material	Application	Performance	Test conditions	Ref.
Cu-BTC/MXene aerogel (P)	Flexible NO_2 sensing	Sensitivity 52.47 (50 ppm), response time 0.9 s	RT (25 °C); RH 23% ± 2%; 5 V DC; 250 mL chamber; PI interdigitated electrode + Au NPs; 50-0.01 ppm; S = R_a/R_g	[103]
Co-TCPP(Fe)/$Ti_3C_2T_x$ (P)	NO gas sensing	limit of detection (LOD) 200 ppb, response time 95 s	Chemiresistive sensor (IDEs on ceramic substrate); 10 ppm NO (N_2 background); RT (30 ± 2 °C); 5-20 V DC; dry N_2; 0.2-10 ppm; S = R_a/R_g; pLOD = 200 ppb	[104]
Cu-HHTP/MXene (P)	Triethylamine sensing	Response time 4 s (50 ppm), 21× sensitivity enhancement	Ag-Pd electrode (14 × 7 mm^2); TEA 1-2,000 ppm; RT; RH < 80%; S = $\|R - R_0\|/R_0$ × 100%; 4/187 s	[66]
Zn/Fe-ZIF/$Ti_3C_2T_x$ (P)	Photocatalytic CO_2 cycloaddition	96% conversion, full-spectrum response	50 mg cat.; 5 mmol ECH + 0.17 mmol TBAB; solvent-free; 1 bar CO_2; Xe lamp full spectrum, 350 mW cm^{-2}; 6 h; GC	[59]
Cu_2[CuTCPP]/Ti_3C_2 (P)	Photocatalytic H_2 evolution	> 5,000 μmol g^{-1}	5 mg cat.; 20 mL water; 150 W Xe lamp, λ > 450 nm; no sacrificial agent; 3 h	[60]
UiO-66-NH_2(Zr/Ti)/MXene (P)	Photocatalytic H_2 evolution	2,187 μmol g^{-1} h^{-1}	10 mg cat.; 100 mL 10 vol% TEOA aq. + H_2PtCl_6 (Pt); 300 W Xe lamp, 350-780 nm; 5 °C ; 5 h	[61]

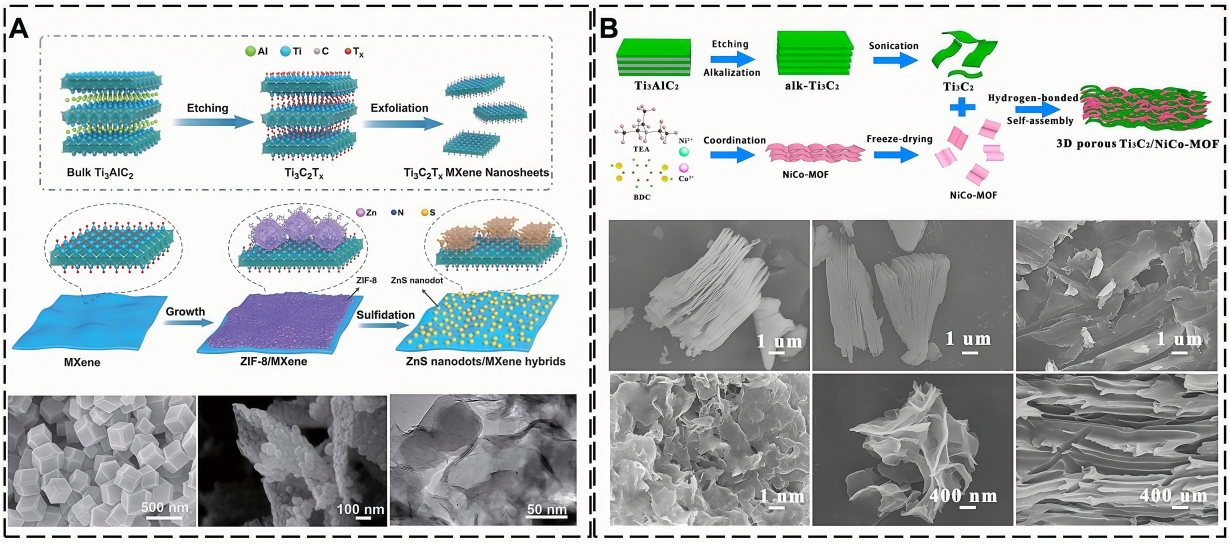


Figure 4. Synthesis strategies of MOF/MXene composites for lithium-ion battery anodes. (A) *In situ* growth of ZnS nanodots/$Ti_3C_2T_x$ MXene hybrids via ZIF-8/MXene precursor followed by sulfidation. Adapted from Ref.[62], under CC BY 4.0 license. (B) Hydrogen-bonded self-assembly of 3D porous Ti_3C_2/NiCo-MOF composite. Adapted from Ref.[105], under CC BY 4.0 license.

MOF/MXene hybrid nanostructures address these limitations by integrating the high surface area, customizable pore channels, and redox-active metal sites of MOFs with the metallic conductivity, hydrophilic terminated surfaces, and mechanical ductility of MXenes [Figure 4].

In situ growth is the dominant preparation technique for LIB anodes, establishing chemical interfacial coupling between MXene substrates and MOF-based active phases. Gao *et al.* proposed an *in situ* conversion strategy derived from LDH precursor growth on MXene sheets, transforming surface-confined LDH into pristine $Ni_{0.8}Mn_{0.2}$ Prussian blue analog (PBA) nanoparticles anchored on $Ti_3C_2T_x$[49]. This *in situ* nucleation mechanism ensures contact between electroactive PBA and the conductive MXene network, delivering a reversible capacity of 442 mAh g^{-1} with high-rate tolerance. Similarly, Xiao *et al.* fabricated 2D/2D $Ti_3C_2T_x$/NiCo MOF heterostructures via solvothermal *in situ* growth, where carboxyl groups on MOF organic linkers form covalent bonds with -OH/-O terminals of MXene, generating heterointerfaces[14]. This interfacial interaction accelerates charge transfer and sustains a capacity of 637 mAh g^{-1} over 200 cycles. However, these studies are typically conducted at low active mass loadings (< 1 mg cm^{-2}), and performance at industrially relevant loadings (> 3 mg cm^{-2}) remains largely unreported.

A critical challenge for alloy-type anode materials (Si, Sn, Sb) lies in extreme volume fluctuation (> 300%) during Li^+ uptake/release, which can be mitigated via spatial confinement enabled by post-synthetic-derived carbon frameworks combined with MXene scaffolds. Zhang *et al.* developed a dual-confinement architecture via MOF carbonization post-treatment: ZIF-8 was first grown *in situ* on MXene surfaces, followed by high-temperature pyrolysis to form nitrogen-doped carbon matrices encapsulating Si nanoparticles, yielding MOF-derived Si/MXene@C hybrids[44]. The MOF-derived carbon buffer layer together with flexible MXene sheets jointly dissipates mechanical strain while retaining conductive pathways, achieving a stable capacity of 1,006.1 mAh g^{-1} over 150 cycles. Similar strategies have been applied to the pristine Sn-MOF/MXene anode (1,009 mAh g^{-1})[43] and the MOF-derived Sb@C/MXene anode (625 mAh g^{-1} over 2,000 cycles)[17], demonstrating the generalizability of this dual-confinement approach. A related conversion-type design, MOF-derived ZnS nanodots anchored on $Ti_3C_2T_x$, likewise achieved stable lithium storage through MXene-confined conversion[62]. Notably, these reversible capacities closely approach—and in the Sn case slightly exceed—the theoretical alloying limits of the metals alone (≈994 mAh g^{-1} for $Li_{4.4}Sn$ and ≈660 mAh g^{-1} for Li_3

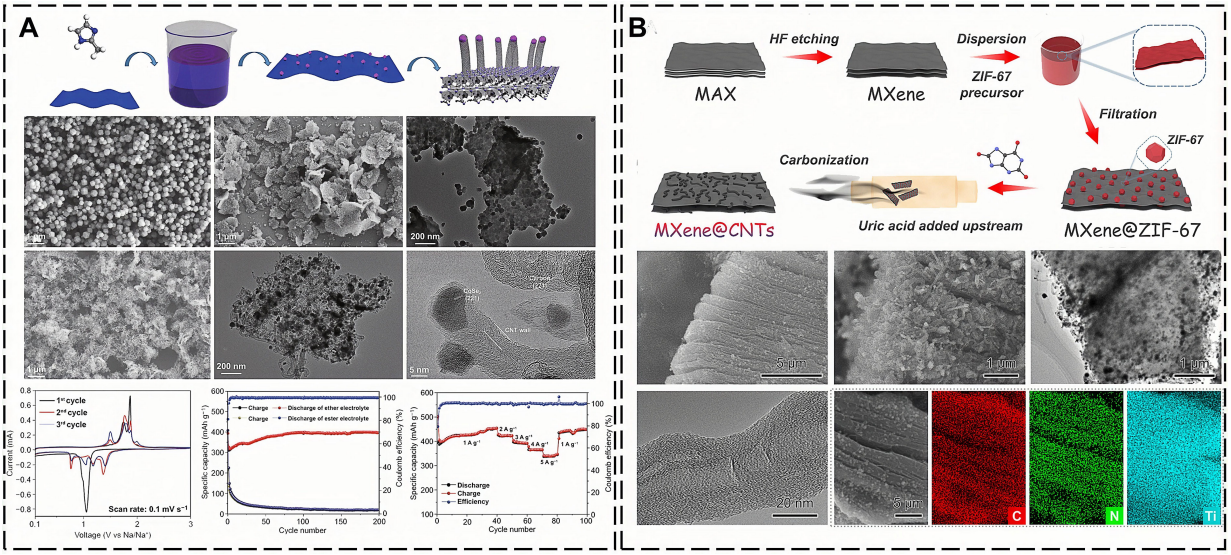


Figure 5. Synthesis strategies of MOF/MXene composites for sodium-ion battery anodes. (A) *In situ* growth of $CoSe_2$@CNTs-MXene via ZIF-67/MXene precursor followed by carbonization and selenization. Adapted from Ref.[110], under CC BY 4.0 license. (B) *In situ* growth of nitrogen-doped carbon nanotubes on MXene nanosheets (MXene@CNTs) via ZIF-67/MXene precursor and uric acid-assisted carbonization. Adapted from Ref.[111], under CC BY 4.0 license.

Sb)[106,107]. The apparent excess for the Sn-based anode is attributable to additional Li^+ storage in the pristine MOF framework (redox-active organic linkers and unsaturated metal nodes), the MXene substrate, and interfacial/pseudocapacitive contributions, and should not be interpreted as exceeding the thermodynamic limit of the full composite.

Beyond the three primary composite strategies, macroscopic structural modulation further optimizes electrode performance. Hydrogen-bonded self-assembly of NiCo-MOF with Ti_3C_2 into a three-dimensional porous network represents another macroscopic strategy for enhancing Li^+ storage[105]. Electrospinning constructs one-dimensional fibrous conductive networks; Chen *et al.* fabricated $Ti_3C_2T_x$@Co fibrous composites that retain a capacity of 422 mAh g^{-1} after 500 cycles[48]. Utilizing intrinsically conductive MOFs provides another pathway: Sun *et al.* built conductive MOF@MXene heterostructures with modulated interfacial electron redistribution, achieving 80% capacity retention after 5,000 cycles[108]. However, the library of intrinsically conductive MOFs remains limited primarily to Cu-, Ni-, and Co-based 2D frameworks, and their chemical stability in carbonate electrolytes is a concern.

The multiple fabrication routes endow MOF/MXene anodes with four key merits: (i) enhanced electronic conductivity via metallic MXene scaffolds; (ii) improved mechanical tolerance toward volume expansion through spatial confinement; (iii) robust interfacial stability from chemical bonding formed during *in situ* growth; and (iv) tunable Li^+ storage kinetics via interface engineering and conductive MOF integration. A critical gap is the lack of standardized testing protocols: most studies report gravimetric capacity at low mass loadings, whereas practical cells require areal capacity > 3 mAh cm^{-2} with electrode thicknesses > 50 μm.

Sodium-ion batteries (SIBs)

SIBs have garnered interest as a cost-effective alternative to lithium-ion technologies, driven by abundant sodium reserves. However, the larger ionic radius of Na^+ (1.02 *vs.* 0.76 Å for Li^+) induces structural stress, sluggish reaction kinetics, and substantial volume expansion during sodiation/desodiation[109] [Figure 5].

A critical advancement in MOF/MXene composite design for SIBs involves hollow hierarchical architectures that buffer mechanical stress. Li *et al.* fabricated MOF-derived hollow MXene@CoS_2/NC composites using MOF/MXene templates followed by nitrogen-doped carbon encapsulation[16]. The hollow interior accommodates volume expansion of CoS_2, while the MXene skeleton ensures continuous electron transport, enabling a reversible capacity of 620 mAh g^{-1} at 0.2 A g^{-1} over 200 cycles. However, the initial Coulombic efficiency of such conversion-type anodes is typically below 80%, and the origin of this irreversibility warrants further investigation. Transition metal phosphides encapsulated within MOF-derived carbon matrices and MXene networks offer alternative high-capacity anodes. Liu *et al.* developed MOF-derived MXene@CoP@NPC composites through phosphorization of ZIF-67 precursors anchored on MXene surfaces[87]. This architecture delivered a stable capacity of 198 mAh g^{-1} at 5 A g^{-1}, demonstrating rate capability essential for high-power applications. Nevertheless, phosphorization processes typically require toxic phosphorus sources, raising safety and environmental concerns for scale-up. Huang *et al.* fabricated MOF-derived Ti_3C_2/CoS_2@NPC composites, achieving a capacity of 282.6 mAh g^{-1} even at 10 A g^{-1}, underscoring the role of pore architecture in facilitating rapid Na^+ diffusion[78]. A dimensional-gradient $CoSe_2$@CNTs-MXene anode prepared from MOF precursors further demonstrated high-capacity, stable sodium storage in ether-based electrolytes[110]. Shi *et al.* introduced a mechanochemical synthesis approach for preparing MOF/MXene composites, representing a sustainable pathway for large-scale manufacturing[112]. However, the uniformity of product distribution on MXene surfaces remains less controlled compared to liquid-phase methods. *In situ* growth of nitrogen-doped CNTs on MXene from ZIF-67 has extended the same conductive-framework concept to dual sodium/potassium storage[111].

A recurring limitation across SIB studies is the use of ether-based electrolytes, which form stable solid electrolyte interphase layers but exhibit lower ionic conductivity than carbonate electrolytes, potentially masking true rate capability[113]. Furthermore, MOF/MXene anodes must be evaluated in full-cell configurations against suitable cathodes to assess true practical viability.

Zinc-based batteries and potassium-ion batteries

MOF/MXene heterostructures address the inherent drawbacks of single-component materials for multivalent and large-radius alkali metal-ion batteries[9]. Pristine MOFs suffer from poor conductivity and fragile frameworks, while pure MXene sheets are limited by insufficient electroactive sites and restacking. The heterointerface shortens ion migration pathways, buffers volumetric variation, and suppresses parasitic side reactions—core bottlenecks restricting cycling lifespan [Figure 6].

Zinc-ion batteries. Aqueous zinc-ion batteries face three obstacles: uncontrolled zinc dendrite nucleation, competitive hydrogen evolution, and irreversible dissolution of cathode active species. For anode protection, Watwiangkham *et al.* combined DFT and molecular dynamics simulations to design $Ti_3C_2O_2$/CuHHB heterointerfaces with strong Zn adsorption affinity and HER suppression. Theoretical calculations verified that the $Ti_3C_2O_2$/CuHHB heterointerface possesses stronger Zn adsorption affinity (0.74 eV higher than water adsorption) and lifts the HER limiting potential to -2.41 V, which theoretically inhibits dendrite growth and parasitic hydrogen evolution[42]. Nevertheless, this work only relies on computational prediction, lacking electrochemical validation to confirm long-term interfacial stability under practical cycling conditions. Different from pure theoretical design, microfluidic 3D printing offers a controllable manufacturing method to construct functional protective layers. Lu *et al.* deposited MXene/Cu-THBQ composite coatings on zinc powder anodes via microfluidic-assisted shaping. This uniform covering homogenizes Zn^{2+} flux distribution and suppresses HER activity, allowing symmetric cells to operate stably for 1,800 h and matching well with organic cathode materials[115]. Despite precise control over coating thickness and component distribution, microfluidic printing suffers from high equipment cost and low batch output, which hinders its large-scale industrial promotion.

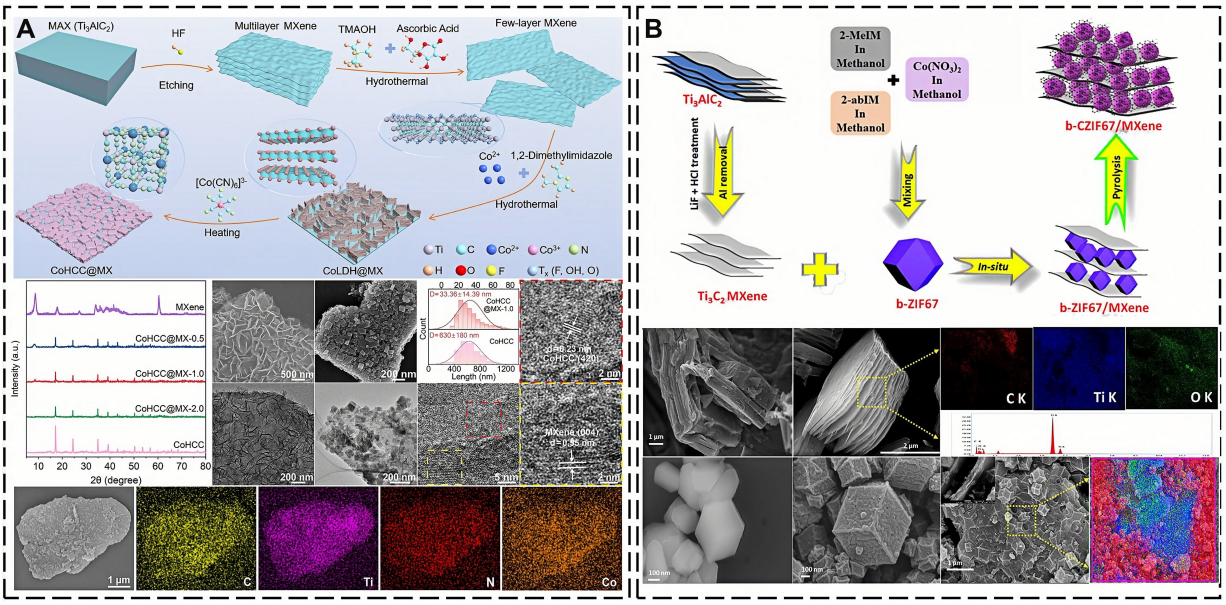


Figure 6. Synthesis strategies of MOF/MXene composites for potassium-ion batteries and zinc-based batteries. (A) *In situ* growth of CoHCC@MX composite via hydroxylated MXene-assisted synthesis for potassium-ion batteries. Adapted from Ref.[63], under CC BY 4.0 license. (B) *In situ* growth of bi-ligand ZIF-67 on MXene followed by pyrolysis to form b-CZIF67/MXene composite for zinc-air batteries. Adapted from Ref.[114], under CC BY 4.0 license.

In terms of zinc-ion battery (ZIB) cathode materials, sandwich-type MOF/MXene heterostructures and MOF-derived carbon-supported metal oxides are two mainstream architectures. Wang *et al.* synthesized a 2D layered pristine Cu-HHTP/MX composite with inherent one-dimensional ion transport tunnels[99]. The MXene substrate remedies the low conductivity of pristine Cu-HHTP MOF, enabling reversible Zn^{2+} intercalation redox reactions. The electrode delivers a specific capacity of 260.1 mAh g^{-1} at 0.1 A g^{-1} and retains 92.5% initial capacity after 1,000 cycles. To further optimize full-cell performance, Sun *et al.* exploited post-synthetic derivation to fabricate MOF-derived Zn/Co co-doped MnO/C microspheres from bimetallic MOF precursors, which were assembled with $Ti_3C_2Cl_2$-modified zinc anodes to construct complete ZIB devices. Dual metal doping relieves Jahn-Teller structural distortion of Mn-based active phases, while the MXene coating on anodes restrains dendrite proliferation. The full cell achieves a capacity retention rate of 98.7% over 3,000 charge-discharge cycles[100]. Hierarchically porous manganese-based ternary composites point to the same conclusion—engineered porosity is central to reversible Zn^{2+} storage—while sharing the same high-loading challenges[116]. A universal deficiency of these MOF-derived cathodes is the capacity decay under high active mass loading; additionally, the high-temperature pyrolysis procedure required for post-synthetic derivation may partially destroy the original porous MOF framework and reduce the number of accessible active sites.

Potassium-ion batteries. Compared with aqueous ZIBs, non-aqueous potassium-ion batteries suffer from more severe volume expansion because K^+ possesses a larger ionic radius than Zn^{2+} and Li^+[117]. MOF/MXene composites fabricated via modified *in situ* growth and dual-confinement strategies have become competitive potassium-ion battery (PIB) anode candidates. For instance, hydroxylated-MXene-assisted *in situ* growth of ultrafine CoHCC nanoparticles produced a high-performance potassium-ion anode[63]. Sun *et al.* proposed a "node-unlocking" interface engineering strategy based on MXene-supported MOF precursors[50]. Selective removal of partial organic linkers exposes abundant metal node sites on NMD-MOF composites, which elevates K^+ adsorption energy and facilitates ion capture. When matched with MD-KVO cathodes, the NMD-MOF anode maintains a reversible capacity of 250 mAh g^{-1}. For conversion-type anode materials with large volumetric strain, Hu *et al.* adopted an *in situ* anchoring route to disperse MOF-derived ZnTe@C 0D

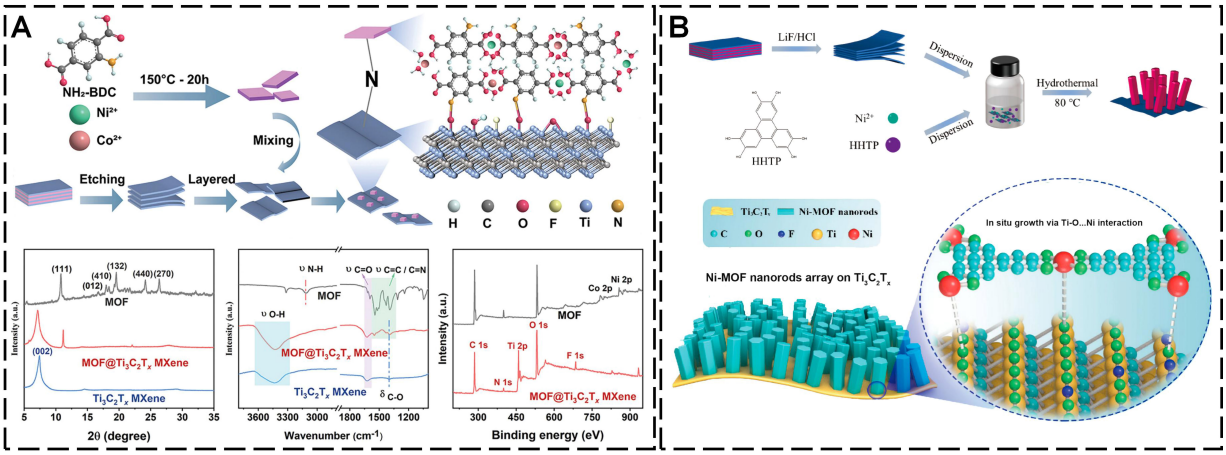


Figure 7. Synthesis strategies of MOF/MXene composites for supercapacitors. (A) Schiff reaction-induced self-assembly of NH_2-Ni/Co-BDC MOF@$Ti_3C_2T_x$ MXene heterostructure. Adapted from Ref.[126], under CC BY 4.0 license. (B) *In situ* growth of Ni-MOF nanorod arrays on $Ti_3C_2T_x$ nanosheets. Adapted from Ref.[127], under CC BY 4.0 license.

nanoparticles over $Ti_3C_2T_x$ MXene nanosheets, constructing 0D/2D dual-confinement heterostructures[45]. The MXene matrix and carbon buffer shell jointly accommodate the structural deformation generated during the reversible conversion reaction ($ZnTe \leftrightarrow Zn + K_xTe_\gamma$). The composite reserves 230.2 mAh g^{-1} after 3,500 continuous cycles. However, all conversion-type MOF/MXene anodes face two common drawbacks: low initial Coulombic efficiency and voltage hysteresis, originating from the slow kinetics of multi-electron redox conversion processes.

Collectively, MOF/MXene heterostructures bring performance improvements to both zinc-based and potassium-ion batteries, yet multiple practical bottlenecks remain unresolved. The intrinsic microporous structure of MOFs blocks the rapid diffusion of large-sized K^+ and hydrated Zn^{2+}; meanwhile, spontaneous restacking of MXene nanosheets during electrode rolling reduces the exposure of heterointerface active sites. Most existing synthesis routes are limited by low productivity and high raw material cost. A further concern is the electrolyte compatibility: non-aqueous PIBs typically use KPF_6 in carbonate solvents, which can react with the surface terminations of MXenes and form resistive surface layers, while aqueous ZIBs operate in mildly acidic electrolytes that may promote MXene dissolution.

Supercapacitors

Market demand for fast-charging, long-lifespan energy storage devices has spurred research on advanced supercapacitor electrode materials. MOF/MXene heterostructures have emerged as a promising direction[118-120]. Conductive MXene sheets act as interconnected current collectors establishing long-range electron transport pathways, offsetting the insulating characteristic of MOF matrices and inhibiting MOF particle aggregation[121-125]. Meanwhile, rigid porous MOF crystals serve as nanoscale spacers between MXene layers, reserving interlayer space for electrolyte permeation and rapid ion intercalation. Interfacial chemical bonds such as Ti-O-Co and Ti-O-Ni are proposed to trigger charge redistribution across heterojunctions, lowering ion desolvation energy and enhancing structural robustness[13,32] [Figure 7].

In situ hydrothermal growth represents the most widely adopted preparation strategy. This route leverages abundant -O, -OH, and -F functional groups on etched MXene surfaces as natural heterogeneous nucleation sites, triggering direct crystallization of MOF nanoparticles or nanosheets on MXene substrates and forming stable covalent bridging bonds at heterointerfaces[128]. The chemical adhesion eliminates loose phase separation frequently observed in mechanically mixed MOF/MXene powders and guarantees uniform

dispersion of redox-active MOF phases over conductive MXene networks. Guo *et al*. proposed a controllable *in situ* anchoring synthesis followed by alkaline etching treatment to fabricate MOF-derived MXene-supported NiCo LDH composites derived from Ni-doped ZIF-67 precursors[13]. XPS-identified Ti-O-Ni interfacial bonds anchor the hydroxides onto negatively charged MXene sheets; the composite exhibits fast cross-interface electron transfer and stable structural buffering during redox cycling, consistent with—though not proving—a bond-mediated pathway. Benefiting from this optimized interfacial coupling, the MXene/NiCoZDH electrode delivers a specific capacitance of 877 F g^{-1} at 1 A g^{-1} and retains 90.9% of initial capacitance after 30,000 continuous charge-discharge cycles[13]. Ni-MOF nanorod arrays grown directly on $Ti_3C_2T_x$ provide freestanding electrodes whose oriented one-dimensional morphology shortens ion-diffusion paths[127]. To systematically reveal metal cation effects on capacitive performance, Ji *et al*. prepared a series of pristine H_3BTC-linked transition metal MOFs (Fe-, Cu-, Co-, Ni-MOF) directly grown on MXene surfaces via identical hydrothermal parameters[71]. Comparative electrochemical characterization combined with DFT theoretical calculations verified that Ni-MOF@MX-2 exhibits the strongest interfacial electronic coupling effect, which accelerates charge transfer kinetics and suppresses structural pulverization. This composite achieves a high capacitance of 1,160.5 F g^{-1} at 1 A g^{-1} with 94% capacity retention after 10,000 cycles. Further interfacial regulation based on hard-soft acid-base theory was realized by Zheng *et al*., who constructed pristine pillared Ni-MOF/Ti_3C_2 composites[15]. These studies demonstrate that *in situ* hydrothermal growth enables strong interfacial bonding and uniform MOF distribution, yet the process is inherently batch-limited and the MOF loading density is often difficult to control independently of crystal size. Additionally, the hydrothermal environment can promote partial oxidation of MXene surfaces, particularly for $Ti_3C_2T_x$ etched with HF, which introduces TiO_2 domains that increase interfacial contact resistance[74,129]. To circumvent this, Schiff-reaction-induced self-assembly has been used to grow NH_2-functionalized Ni/Co-BDC MOFs on $Ti_3C_2T_x$ under non-hydrothermal conditions[126].

To overcome the poor structural ordering and low batch productivity of traditional hydrothermal batch synthesis, microfluidic assembly and coaxial electrospinning have emerged as advanced continuous manufacturing techniques, providing precise morphological control over fiber-shaped and freestanding flexible supercapacitor electrodes. These processing methods expand the practical application scope of MOF/MXene composites toward wearable and textile energy storage devices. Zhang *et al*. pioneered microfluidic channel synthesis to fabricate core-shell ZIF-67@$Ti_3C_2T_x$ fibrous electrodes[128]. Within confined microfluidic flow channels, MXene nanosheets self-assemble into continuous conductive fiber skeletons, while ZIF-67 polyhedrons uniformly anchor on fiber surfaces through *in situ* coordination reactions. The regularly arranged pore channels inside fibers shorten ion diffusion distances and realize rapid cross-component electron transmission. The resultant fiber electrode reaches an ultrahigh volumetric capacitance of 972 F cm^{-3} and maintains 90.8% performance after 20,000 bending cycles, far outperforming conventional slurry-cast rigid electrodes. Building upon this microfluidic framework, Wu *et al*. designed core-sheath ZIF-L(Zn)@$Ti_3C_2T_x$ fibers with Ti-O-Zn and Ti-F-Zn dual interfacial bonds[39]. The flexible fibrous network can be woven into stretchable capacitive fabrics, delivering a volumetric capacitance of 1,700 F cm^{-3} with exceptional cyclic endurance over 20,000 runs. Coaxial electrospinning serves as another complementary scalable route to construct self-supporting electrode films without extra polymer binders. Pathak *et al*. prepared hollow MXene-containing carbon nanofibers via coaxial spinning, sequentially modifying fiber surfaces with polypyrrole conductive layers and immobilized ZnCoMOF nanoparticles[118]. The interconnected three-dimensional conductive network eliminates MXene restacking and establishes dual transport channels for ions and electrons. However, the mass loading of active MOF materials in microfluidic and electrospun fibers is typically lower than in slurry-cast electrodes, which limits the overall areal capacitance. The trade-off between fabrication scalability and energy density remains a key engineering challenge for these advanced processing methods.

Post-synthetic thermal and chemical treatment converts as-prepared MOF/MXene precursors into high-conductivity metal compounds including oxides, hydroxides, sulfides, and phosphides, while inheriting the original hierarchical porous morphology of MOF templates. This strategy fundamentally addresses the intrinsic low conductivity of pristine MOF frameworks. Yang *et al*. adopted mild low-temperature thermal annealing to modulate Ti-O-Co bridging bond density within Co-BDC/$Ti_3C_2T_x$ 2D/2D heterostructures[32]. Controlled heating optimizes interfacial electronic coupling without destroying the original layered heterostructure, generating substantially improved capacitive performance compared with unannealed raw composites. Multi-step bottom-up self-assembly and top-down chemical etching enable precise construction of porous nickel phosphate supported on MXene substrates, as reported by Zhang *et al*.[84]. MOF-derived nickel phosphate possesses high theoretical pseudocapacitance, yet its poor bulk conductivity limits practical performance; the underlying MXene conductive network solves this bottleneck and reserves hierarchical pores formed during etching, delivering a charge capacity of 639 C g^{-1} with 85% retention after 10,000 cycles. *In situ* sulfurization of MOF/MXene hybrids is widely used to synthesize metal sulfide active phases with abundant redox states. Ruan *et al*. converted MXene-supported ZIF-67 into dendritic $CoNi_2S_4$ wrapped by continuous MXene sheets via high-temperature sulfur vapor treatment[92]. The dendritic nanostructure maximizes exposed redox-active surfaces, while MXene wrapping guarantees rapid charge collection and mechanical protection, reaching a specific capacity of 933 C g^{-1}. CoS/Ti_3C_2 heterostructures were further shown to accelerate redox kinetics for high-rate supercapacitor electrodes[65]. Ion exchange combined with sulfidation further creates advanced yolk-shell structured $NiCo_2S_4$@Co_3S_4 nanocages anchored on $Ti_3C_2T_x$ substrates for asymmetric supercapacitor positive electrodes[79]. These derivatives demonstrate that post-synthetic conversion can significantly boost conductivity, yet the trade-off is a loss of crystalline MOF porosity and a potential increase in MXene oxidation. The structural complexity of the final product also makes it difficult to establish precise structure-performance correlations, as the electrochemical response may originate from multiple components (residual MOF, derived metal sulfide, oxidized MXene, and carbon matrix) rather than a well-defined interface[130].

Unlike traditional insulating MOFs that demand carbonization or conductive additives, π-conjugated conductive MOFs deliver intrinsic in-plane electron transport capacity, simplifying electrode composition and elevating volumetric capacitance. Zhu *et al*. fabricated MXene@Ni-HHTP composite electrodes by assembling two-dimensional conductive Ni-hexahydroxytriphenylene MOF nanosheets with $Ti_3C_2T_x$ substrates[18]. The fully conjugated ligand framework of Ni-HHTP offers continuous intramolecular conductive channels, while MXene layers suppress mutual restacking of conductive MOF sheets and enhance overall mechanical toughness. This hybrid material realizes a capacitance of 416.6 F g^{-1} when matched with capacitive negative electrodes in asymmetric devices and exhibits rate tolerance under high current loads. To further regulate interfacial charge injection dynamics, Singha *et al*. inserted ultrathin h-BN dielectric nanosheets as intermediate layers between MOF-derived carbon and MXene phases, constructing ternary MOF-MXene-BN heterostructures[38]. Distribution of relaxation times characterization confirms that the h-BN interlayer optimizes charge migration and inhibits direct chemical corrosion between the two functional components. The sophisticated ternary heterostructure achieves a high charge capacity of 798 C g^{-1} and an energy density of 81 Wh kg^{-1}, retaining 81% capacitance after 5,000 cycles[38]. Recent work further extends these designs to multifunctional electrodes combining supercapacitive storage with electrocatalytic CO_2RR and to bimetallic Ni-Mo-MOF electrodes serving both supercapacitors and the OER[55,56]. Device-level demonstrations are also emerging: MXene-integrated MnCo bimetallic MOF hybrids retain capacitive performance in solid-state configurations, and template-assisted NiCo-MOF/MXene nanocomposites operate in both symmetric and asymmetric hybrid devices[131,132]. However, the practical popularization of conductive MOF/MXene composites is restrained by two key barriers: the limited library of available conductive MOF species (primarily Ni-HHTP, Cu-HHTP, and a few Fe-based frameworks) and complicated ligand synthesis procedures that increase material preparation difficulty and raw material cost. Furthermore,

the chemical stability of conductive MOFs in aqueous acidic or alkaline electrolytes is generally inferior to that of conventional ZIFs or carboxylate MOFs.

Several technical bottlenecks still hinder the commercial translation of MOF/MXene supercapacitor electrodes. First, the dominant microporous structure (< 2 nm) of most MOF building blocks impedes rapid diffusion of large-sized solvated ions in organic and ionic liquid electrolytes, generating high interfacial charge transfer resistance and deteriorating high-rate performance. This issue is particularly acute for asymmetric devices using ionic liquid electrolytes, where the solvated ion size can exceed 1 nm, approaching the micropore limit of typical MOFs. Second, even with MOF nanospacers inserted between MXene layers, weak van der Waals attraction still drives partial restacking of MXene nanosheets during electrode rolling and long-term cyclic operation, gradually reducing the number of available heterojunction active sites. Moreover, most reported high-performance electrodes are tested at low active mass loadings (< 2 mg cm^{-2}) in laboratory conditions; performance attenuation becomes obvious when scaling up electrode thickness to meet practical device energy demands[133]. A systematic evaluation of MOF/MXene supercapacitor electrodes at loadings > 5 mg cm^{-2} and in pouch-cell configurations is largely absent from the current literature. Fourth, the cost of MOF precursors and the complexity of MXene etching and delamination remain significant barriers to industrial-scale manufacturing. High-purity MXene production currently requires multi-step liquid-phase exfoliation with hazardous HF or LiF/HCl mixtures, which raises environmental and safety concerns for factory-scale implementation.

Electrochemical catalysis

Driven by the demand for low-cost, durable electrocatalysts to advance renewable energy conversion technologies, MOF/MXene heterostructures have emerged as a material platform to substitute scarce noble metal catalysts such as Pt, RuO_2, and IrO_2[134]. Single-component electrocatalysts suffer inherent performance bottlenecks that can hardly be overcome independently. Rational hybridization of MOFs and MXenes constructs complementary heterointerfaces and unlocks synergistic catalytic effects unavailable to single-phase materials[19,33,58,135]. MXene nanosheets act as interconnected conductive skeletons to establish uninterrupted electron highways and suppress MOF particle agglomeration, while porous MOF frameworks provide exposed catalytic centers and channels for electrolyte penetration and reactant mass transfer. Interfacial interactions ranging from electrostatic attraction to covalent bonding modulate the electronic structure of active sites and can lower the activation energy for rate-determining steps.

As summarized in Section "STRATEGIES OF MOF/MXene COMPOSITING", each synthesis route delivers distinct interfacial bonding states, morphological characteristics, and catalytic advantages for MOF/MXene composites. *In situ* liquid-phase growth directly induces MOF nucleation on MXene surfaces relying on surface -O, -OH, -F anchoring groups, achieving tight solid-liquid derived heterointerfaces[33,67,69]. Zhao's group adopted an interfacial diffusion-controlled strategy to grow 2D CoBDC nanosheets uniformly on $Ti_3C_2T_x$ substrates, realizing homogeneous heterostructure construction without phase separation[33]. Electrostatic self-assembly takes advantage of negatively charged MXene sheets and positively charged pre-synthesized MOF nanosheets to build ordered 2D/2D superlattices with maximized contact area[80]. Post-synthetic thermal or chemical conversion represents the most widely adopted method to boost intrinsic catalytic activity: MOF/MXene precursors are transformed into metal phosphides, sulfides, or metal-carbon composites while retaining the original hierarchical framework[24,136]. Zong *et al.* converted ZIF-67/Ti_2NT_x hybrids into CoP/MXene electrocatalysts via low-temperature phosphorization, while Murtaza's team realized CoP/C@Nb_2CT_x heterostructures through sequential carbonization and phosphorization treatments[23,89]. Supplementary advanced interfacial tuning tactics include electrochemical deposition for ultrathin MOF film coating and dual-ligand modification to strengthen MOF structural flexibility after compositing with MXene substrates[137]. However, a critical limitation of all four strategies is that the

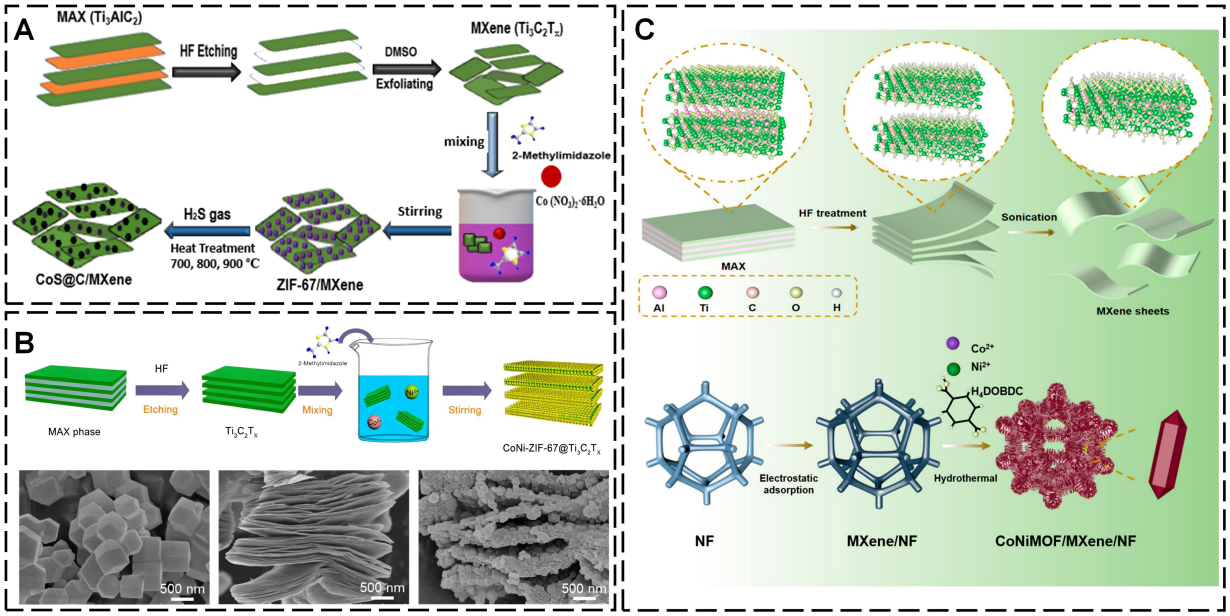


Figure 8. Synthesis strategies of MOF/MXene composites for electrocatalysis. (A) Post-synthetic sulfidation of ZIF-67/MXene precursor to form CoS@C/MXene nanocomposites at different temperatures. Adapted from Ref.[138], under CC BY 4.0 license. (B) *In situ* growth of CoNi-ZIF-67 rhombic dodecahedrons on $Ti_3C_2T_x$ MXene via a coprecipitation reaction. Adapted from Ref.[139], under CC BY 4.0 license. (C) Electrostatic adsorption of MXene on nickel foam (NF) followed by hydrothermal growth of Ni-doped Co-MOF-74 to form CoNi-MOF-74/MXene/NF. Adapted from Ref.[64], under CC BY 4.0 license.

resulting catalytic sites are often heterogeneous and poorly characterized: the active phase may include residual MOF fragments, derived metal compounds, MXene edge sites, and interfacial coordination complexes, making mechanistic attribution difficult [Figure 8].

MOF/MXene heterostructures exhibit catalytic efficiency toward diverse electrocatalytic reactions, starting with the ORR critical to fuel cells and rechargeable metal-air batteries. Commercial Pt-based ORR catalysts face high cost and methanol crossover poisoning issues, whereas MOF/MXene hybrids with atomically dispersed M-N_x active sites deliver comparable catalytic activity and superior stability. Wang *et al.* fabricated MOF-derived Fe-N-C@$Ti_3C_2T_x$ composites via stepwise pyrolysis of Fe-doped ZIF-8 grown on MXene surfaces[19]. Strong heterojunction coupling reduces charge transfer resistance, affording half-wave potentials of 0.887 V in alkaline media and 0.777 V in acidic electrolytes, with negligible activity decay after over 10,000 continuous potential cycles[19]. Gu and coworkers anchored NH_2-MIL-53(Fe)-derived Fe-N_x single atoms on Ti_3C_2 MXene; the negatively charged MXene surface restrains thermal aggregation of Fe species, modulates the d-band electronic configuration of isolated Fe sites, and strengthens tolerance to methanol cross-contamination relative to commercial Pt/C[135]. Such systems validate that MXene conductive supports stabilize atomic catalytic centers and accelerate the four-electron ORR pathway. However, the turnover frequency (TOF) of these Fe-N_x sites and their site density remain incompletely quantified, making it difficult to assess whether the observed activity originates from true single-atom sites or from small clusters. Furthermore, the stability of M-N_x motifs under acidic ORR conditions is questionable, as protonation and demetalation can occur during extended operation, a phenomenon that is rarely monitored in laboratory studies.

The OER constitutes the anodic half-reaction of water splitting and metal-air batteries, which requires catalysts stable under high oxidative potentials and capable of lowering four-electron transfer barriers. OER is also the application in which the pristine/derived distinction is least meaningful at the operating stage, because both types of precursors converge on the same working phase. Pristine MOF/MXene

systems—including the diffusion-grown CoBDC/$Ti_3C_2T_x$ 2D/2D heterostructure (1.64 V *vs.* reversible hydrogen electrode at 10 mA cm^{-2} in 0.1 M KOH, Tafel slope 48.2 mV dec^{-1})[33], the $Fe_{2.1}Ni_{0.7}Co_{0.2}$-MIL-88A/$Ti_3C_2T_x$ composite (overpotential 231 mV at 10 mA cm^{-2}, TOF 2.33 s^{-1})[57], electrodeposited CoFe bimetallic MOF nanosheets on monolayer MXene (overpotential 191 mV, Tafel slope 31 mV dec^{-1})[58], electrostatically assembled Co_2Ni-MOF/$Ti_3C_2T_x$[80], and dual-ligand modified Co-MOF/MXene frameworks[137]—are crystalline in the as-prepared state, but their metal centers are converted *in situ* to metal (oxy)hydroxides under anodic polarization. The same reconstruction occurs for MOF-derived systems such as NiCoS/MXene obtained by post-synthetic sulfidation and CoNi-ZIF-67/$Ti_3C_2T_x$ composites[85,139]. The MOF thus acts only as a sacrificial precursor that delivers dispersed metal sites and a porous scaffold, while the MXene supplies the conductive network and stabilizes the reconstructed layer. For this application the materials are therefore classified by their working phase rather than by the crystallinity of their MOF precursor, and performance is attributed to the (oxy)hydroxide/MXene interface, not to the MOF. A critical issue is that the reported current densities are universally below 100 mA cm^{-2}, and the durability of these reconstructed catalysts at higher current densities remains essentially unknown.

For the cathodic HER of water electrolysis, MOF/MXene heterojunctions and post-converted metal phosphide/sulfide derivatives achieve catalytic performance across both acidic and alkaline environments. Tiwari constructed a pristine covalently bonded $Ni_3(HITP)_2$-MOF/$Ti_3C_2T_x$ via Ti-N linkages; strong interfacial electron transfer optimizes hydrogen adsorption free energy on metal sites, achieving overpotentials of 180 mV in alkaline media (1.0 M KOH) and 240 mV in acidic conditions (0.5 M H_2SO_4)[140]. MXene-supported MoNiS derived from MOF precursors balances intermediate adsorption and avoids MXene oxidative corrosion, reaching an overpotential of 153 mV with a Tafel slope of 92 mV dec^{-1} in 1 M KOH[136]. Similarly, MOF-derived cobalt sulfide/carbon nanocomposites on MXene have been reported as bifunctional OER/HER catalysts[138]. Murtaza's CoP/C@Nb_2CT_x obtained by sequential carbonization and phosphorization is bifunctional, realizing HER and OER overpotentials of 50 and 149 mV, respectively, at 10 mA cm^{-2} in 0.1 M KOH, standing out among non-noble metal phosphide electrocatalysts[89]. For translation to practice, the more informative benchmark is the full-cell demonstration recently provided by scalable electrodeposited NiMoP, which follows catalyst performance through to alkaline electrolyzer operation[141]. It should be noted that direct comparison of overpotentials is strictly valid only within the same electrolyte system, as different pH values and electrolyte compositions significantly affect reaction kinetics. Additionally, oxygen-vacancy-enriched Ce-MOF/MXene delivers bifunctional HER/OER activity and stable cycling, expanding the application boundary of single-component hybrid catalysts[142]. However, the MXene surface can undergo oxidation and dissolution under prolonged cathodic polarization in acidic electrolytes, which is rarely addressed at present. The stability data for HER catalysts are typically limited to < 100 h of chronopotentiometry, which remains far below the stack lifetimes of commercial alkaline (50,000-96,000 h) and proton-exchange-membrane (70,000-100,000 h) electrolyzers[143]. For reference, alkaline electrolyzers operate at current densities of 0.25-0.45 A cm^{-2} and proton-exchange-membrane electrolyzers at 1.0-2.0 A cm^{-2}[144].

Developing bifunctional and trifunctional electrocatalysts capable of driving multiple reactions simultaneously simplifies electrolyzer and battery device assembly and cuts manufacturing costs. Zong's Ti_2NT_x-wrapped ZIF-67-derived CoP composite serves as a bifunctional catalyst for overall water splitting, with HER overpotential of 112 mV, OER overpotential of 241 mV, and a full-cell voltage of 1.61 V at 10 mA cm^{-2}, exceeding the simple performance superposition of individual catalysts[23]. Trimetallic BTC-derived NiCoCuO/MXene further reduces overall water splitting voltage to 1.38 V due to multi-valence electronic modulation, outperforming commercial Pt/C||IrO_2 paired electrodes[101]. Ni-doped Co-MOF-74 grown on MXene-coated nickel foam provided a self-supported electrode for overall water splitting[64]. Multi-functional catalysts integrating HER, OER, and ORR are suitable for regenerative zinc-air batteries[114]. He's

CoO_x-N-C/TiO_2-C/MXene trifunctional hybrid achieves a water splitting voltage of 1.45 V and a narrow potential gap between ORR and OER, showing value for integrated energy storage-conversion devices[145]. An MXene-supported MOF-derived CoP nanocomposite has subsequently been shown to combine OER, HER, and ORR activity in a single catalyst[90]. It is important to note that bifunctional and trifunctional metrics are typically evaluated in separate half-cell configurations using different electrolytes; the true simultaneous catalytic performance in a single electrolyte environment (e.g., 1 M KOH for both HER and OER) often yields lower performance than the sum of individual half-cell values due to competing surface reconstruction processes. The mechanical stability of MOF/MXene catalyst layers during gas evolution (bubble detachment stress) is also rarely evaluated, yet it is a critical factor for membrane electrode assembly durability.

Beyond water electrolysis and air battery catalysis, MOF/MXene composites display performance in emerging electroreduction and small-molecule conversion fields. Electrochemical CO_2RR relies on MOF porous channels to concentrate CO_2 molecules and MXene conductive networks to deliver electrons, yet material selectivity and long-term stability remain major obstacles[7,10]. For ambient NRR, ZIF-67/$Ti_3C_2T_x$ composites supply abundant Lewis acidic Co sites to activate N≡N triple bonds, attaining an ammonia yield of 6.52 μmol h^{-1} cm^{-2} and a Faradaic efficiency of 20.2%[102]. It should be noted that although this value is reported by the cited study, the electrocatalytic NRR community widely acknowledges the risk of false-positive NH_3 signals due to ambient nitrogen contamination. Therefore, rigorous control experiments, such as $^{15}N_2$ isotope-labeled tests, are highly recommended to confirm the origin of the produced ammonia and to verify the reliability of such high Faradaic efficiency values. When applied to fuel cell anodic MOR, ZIF/$Ti_3C_2T_x$ supported ultra-fine Pt nanoparticles deliver a mass activity of 1,900.1 mA mg^{-1} and anti-CO poisoning capacity[146]. MXene substrates also effectively protect HKUST-1 MOF frameworks from high-temperature hydrothermal decomposition and endow MOF-derived Ni nanoparticles with catalytic activity for solid-state hydrogen storage[20]. However, the TOF and mass activity values for Pt-based catalysts in MOR are often obtained under specific experimental conditions (e.g., scan rate, Pt loading) that are not standardized across studies, making direct comparison problematic[147].

Future research can break through the limitations of MOF/MXene composites, including the ease of oxidation of MXene and collapse of the MOF skeleton, through five targeted directions. First, researchers should expand the MXene material library beyond conventional $Ti_3C_2T_x$ to Nb_2CT_x, $Mo_2TiC_2T_x$, and $Mo_2Ti_2C_3$ series with enhanced anti-oxidation performance and tunable electronic structures. Second, machine learning and high-throughput computational screening can be adopted to predict optimal MOF-MXene matching pairs and interfacial charge transfer behaviors, reducing experimental trial-and-error cycles. Third, operando synchrotron X-ray absorption spectroscopy, *in situ* Raman, and TEM characterization must be widely utilized to capture dynamic structural reconstruction and active site evolution during real electrocatalytic processes, clarifying reaction mechanisms. Fourth, scalable green manufacturing technologies including continuous flow synthesis and electrochemical exfoliation should be developed to realize large-area electrode mass production. Finally, catalyst performance must be systematically validated in practical membrane electrode assemblies and flow electrolytic cells, narrowing the gap between lab testing indicators and industrial application standards. Systematic breakthroughs in these aspects will exploit the multi-functional catalytic potential of MOF/MXene heterostructures and accelerate the commercialization of low-cost electrocatalytic energy conversion technologies.

Sensing applications

The hybridization of MOFs and two-dimensional MXenes has been widely accepted for sensing technology, overcoming the performance limits of individual sensing materials and generating synergistic signal transduction effects[103,148-150]. Chemiresistive gas sensors represent a mature application direction of MOF/MXene composites, which can operate at room temperature and avoid the high energy consumption

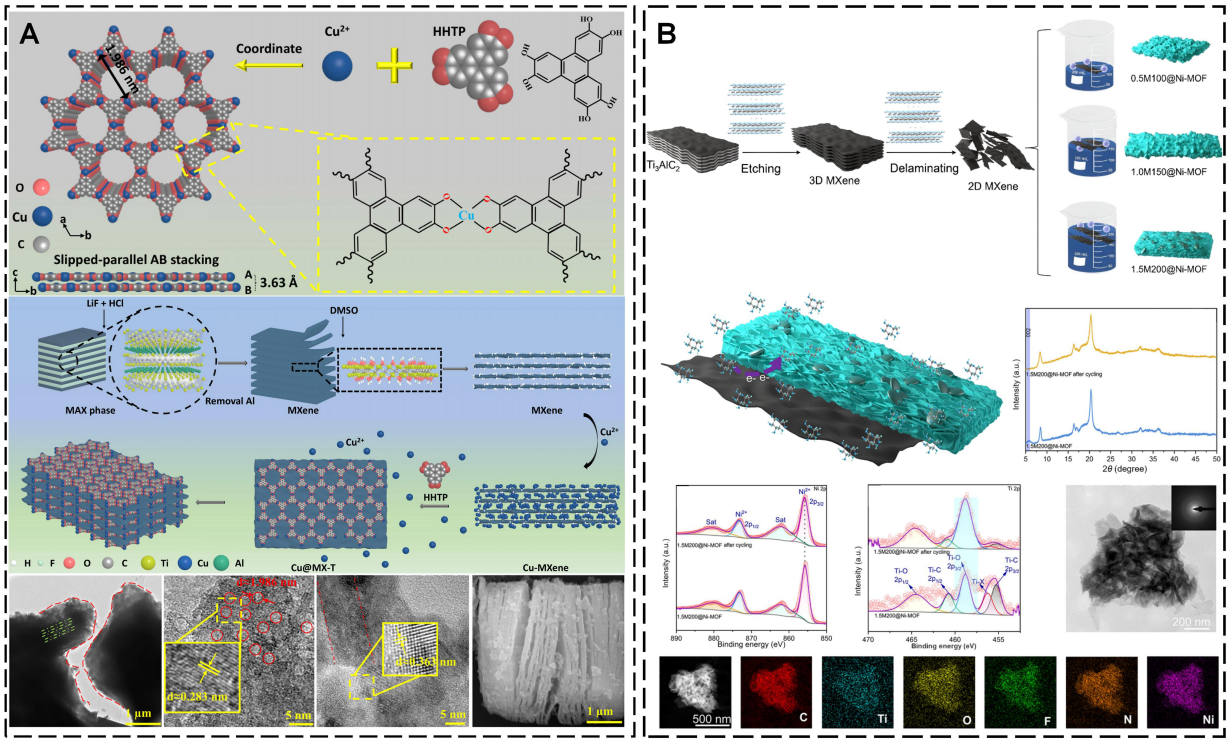


Figure 9. Synthesis strategies of MOF/MXene composites for sensing applications. (A) *In situ* growth of Cu-HHTP MOF within MXene interlayers to form MXene@Cu-HHTP heterostructure for triethylamine sensing. Adapted from Ref.[66], under CC BY 4.0 license. (B) *In situ* growth of Ni-MOF on MXene for glucose sensing. Adapted from Ref.[153], under CC BY 4.0 license.

of traditional high-temperature metal oxide gas detectors. A series of heterostructures fabricated via etching, self-assembly, and MOF template conversion have been developed for trace detection of toxic, volatile gaseous pollutants. For low-concentration NO_2 monitoring, Liu *et al.* prepared Cu-BTC/MXene conductive aerogels via solvent-assisted selective pore etching followed by hydrogen-bond-driven self-assembly[103]. Defect-rich open micropores derived from controlled etching supply gas adsorption sites, and continuous hydrogen-bond-connected MXene conductive pathways boost resistance variation signals upon NO_2 adsorption. The composite sensor delivers a response value of 52.47 toward 50 ppm NO_2 with response/recovery durations of 0.9 and 4.5 s, respectively[103]. To further utilize MOF as a structural sacrificial template, Peng *et al.* adopted hydrothermal growth and aging treatment to deposit CuO nanoparticles on MXene substrates, retaining the high porosity inherited from MOF precursors while generating heterojunction interfaces to enhance gas response. This device realizes NO_2 detection with a 30 ppb limit of detection (LOD) and stable signal output over 10 consecutive weeks[151]. For ammonia sensing vulnerable to humidity interference, ZIF-67 modified via ligand exchange was self-assembled with $Ti_3C_2T_x$ to construct hydrophobic H-MOF/MXene composites. Optimized surface hydrophobicity suppresses water molecule competitive adsorption; even under 76% and 93% relative humidity, signal attenuation only reaches 0.22% and 0.27%, with a theoretical ammonia detection limit as low as 12.8 ppb[152]. In addition, porphyrin Co-TCPP(Fe) MOF was combined with MXene to form Schottky heterointerfaces for trace NO identification, restoring Fe-N_4 active sites to capture nitric oxide and reaching a 200 ppb detection threshold with response/recovery times of 95 and 15 s[104]. Sandwich layered conductive Cu-HHTP/MXene heterostructures further expand gas detection targets to triethylamine, featuring an ultra-rapid 4 s response at 50 ppm and stable performance under 80% humidity environments[66]. These studies demonstrate that MOF/MXene gas sensors achieve detection limits in the ppb range, yet most evaluations are conducted in dry synthetic air. Real-world applications involve complex gas mixtures with varying humidity and temperature, conditions under which MOF frameworks may undergo structural rearrangement or competitive adsorption that degrades selectivity. The long-term drift of baseline resistance in MOF/MXene sensors (> 6 months) is also rarely reported, which is a critical parameter for industrial deployment [Figure 9].

Electrochemical sensing based on MOF/MXene hybrid electrodes covers environmental heavy metal detection, food residue analysis, and biomedical small molecule quantification, combining the electrocatalytic activity of MOF metal sites and fast electron transfer networks of MXenes. For neurotransmitter dopamine testing, Zn-MOF was directly compounded with Ti_3C_2 MXene to overcome the insulating limitation of pure MOFs, enabling dopamine quantification with a detection limit of 110 nM[148]. By switching the MXene substrate to $Nb_4C_3T_x$ and adopting full *in situ* MOF growth, Boruah *et al*. further strengthened target molecule affinity on electrode surfaces, realizing an LOD of 0.2 nM and a linear detection window ranging from 1 to 100 nM[154]. In the field of food safety antibiotic monitoring, one-pot hydrothermal *in situ* growth of CoFe-MOF on MXene-modified hydrophobic carbon paper provides catalytic sites for chloramphenicol redox reactions, achieving picomolar-level 33 pM detection sensitivity[155]. ZIF-67-derived bimetallic LDH electrostatically assembled with MXene creates a wide linear range (0.079-521 μM) for ciprofloxacin identification with a 0.013 μM detection limit[156]. Mycotoxin aflatoxin B1 detection relies on covalent antibody immobilization on Mo-MOF/Ti_3C_2 composites; combined with electrochemical impedance spectroscopy measurement, the sensor achieves an LOD of 8 pg/mL within a linear interval of 0.06-50 ng/mL[157]. For environmental heavy metal pollution control, one-step hydrothermal synthesized Fe-MOF/MXene forms strong hydroxyl-As binding sites to capture As(III), reaching a detection limit of 0.58 ng L^{-1}[158]. Flower-shaped Cu-MOF/MXene and calcined Ni-MOF-derived NiO/MXene both serve as non-enzymatic hydrogen peroxide sensing electrodes: the former utilizes Cu-based catalytic centers to attain a 0.35 μM LOD, while the three-dimensional porous framework of the latter effectively prevents MXene sheet stacking during repeated operation[150,159]. The conductive MOF-on-MXene architecture has also been applied to non-enzymatic glucose detection[153]. Despite these low detection limits, most electrochemical sensors are validated in buffer solutions containing only the target analyte. The performance in real matrices such as blood serum, food extracts, or wastewater is rarely reported, and electrode fouling by proteins, lipids, or surfactants can severely degrade the practical utility of these devices. Furthermore, the reproducibility of sensor fabrication-particularly the uniformity of MOF coating on MXene surfaces-remains a significant challenge, with batch-to-batch variation in sensitivity often exceeding 15% in reported studies.

Benefiting from the intrinsic flexibility and good biocompatibility of MXene substrates and tunable biological ligand environments of MOFs, MOF/MXene composites have achieved progress in biological analysis and wearable real-time health monitoring. For ultrasensitive extracellular vesicle detection, CuNi bimetallic MOF was hybridized with MXene quantum dots to construct label-free aptasensors[160]. The large specific surface of bimetallic MOFs immobilizes abundant aptamer recognition fragments, while MXene quantum dots accelerate interfacial electron exchange, supporting trace exosome quantification down to 5 particles μL^{-1}. For wearable point-of-care melatonin monitoring, biocompatible Zn-glutamate bio-MOF was grown on Nb_2CT_x-coated carbon yarn electrodes, which can be fabricated into adhesive bandage-style wearable sensors with a detection limit of 215 nM for real-time body fluid analysis[161]. Beyond conventional biomedical testing, this composite sensing system has also been applied to cultural heritage protection research: MXene/CNT/MOF hybrid electrodes realize ultrasensitive collagen detection for archaeological leather relic identification, with a detection limit as low as 83 pg/mL, opening a sensing application direction rarely reported in previous literature[162]. However, the long-term stability of wearable sensors under continuous skin contact, sweat exposure, and mechanical deformation remains largely uncharacterized. The biodegradation of MOF frameworks in physiological fluids and the potential cytotoxicity of MXene nanosheets are safety concerns that must be addressed before clinical translation. The issue of non-specific binding in complex biological fluids, which can generate false-positive signals, is also insufficiently addressed in most reported studies.

Apart from single-target single-mode sensors, MOF/MXene heterostructures can be designed into integrated multifunctional systems that couple sensing performance with energy harvesting or structural monitoring. MXene/MOF-derived carbon foam integrates piezoresistive structural health monitoring[163]. The material

delivers a piezoresistive sensitivity of 1.98 kPa^{-1}, serving as a real-time deformation monitoring sensor. Semiconductor $Ni_3(HITP)$ conductive MOF composited with MXene forms flexible temperature sensing electrodes[164]. The composite possesses a temperature coefficient of resistance of -3.1% $°C^{-1}$, supporting continuous human body temperature and respiration monitoring with 0.1 °C measurement accuracy. Self-powered gas sensing platforms eliminate external power supply by combining triboelectric nanogenerators with $Ti_3C_2T_x$/MOF-derived CuO heterostructures. Triboelectric energy generated by mechanical deformation drives ammonia detection, and the sensor reaches a response value of 24.8 under 100 ppm ammonia atmosphere without extra power input[165]. These multifunctional systems represent creative extensions of MOF/MXene composites, though the integration of multiple functions often comes at the expense of sensing selectivity and response speed, as the non-sensing components may introduce additional background noise or interference. The energy conversion efficiency of triboelectric nanogenerators integrated with MOF/MXene sensors is typically below 10%, which may be insufficient for powering data transmission modules in practical IoT applications.

Photochemical catalysis

Photocatalytic water splitting for hydrogen evolution stands as the most extensively studied application of MOF/MXene photocatalysts, where controlled interfacial bonding significantly boosts hydrogen output. Shi constructed UiO-66-NH2(Zr/Ti)/MXene heterostructures via coordination assembly; carboxyl groups strengthen interfacial contact and promote water dissociation, achieving a 20-fold higher H_2 generation rate (2,187 μmol g^{-1} h^{-1}) relative to pristine MOF[61]. Li further realized Ti-N-linked MIL-NH_2/Ti_3C_2 composites through *in situ* MXene-derived growth, which shortens electron migration paths and delivers a hydrogen evolution rate of 4,383.1 μmol h^{-1} g^{-1}[166]. Multi-interfacial Ti_3C_2/TiO_2/UiO-66 ternary heterostructures fabricated by thermal annealing create cascade charge transfer channels, yielding a hydrogen production rate of 1,980 μmol h^{-1} g^{-1}[167]. Exfoliation-assembled 2D/2D Cu_2[CuTCPP]/Ti_3C_2 Schottky junctions maximize built-in electric fields, realizing a H_2 yield over 5,000 μmol g^{-1} after 3 h of irradiation and enabling unassisted overall water splitting without sacrificial reagents[60]. These studies demonstrate that interfacial engineering is critical for photocatalytic performance, yet the hydrogen evolution rates are still orders of magnitude lower than those of benchmark semiconductor photocatalysts such as CdS and g-C_3N_4 when normalized to surface area[168]. Furthermore, the stability of MXene under continuous illumination is questionable, as photoexcited carriers can catalyze the oxidation of $Ti_3C_2T_x$ to TiO_2, leading to progressive degradation of the conductive scaffold [Figure 10]. Where apparent quantum yield (AQY) values are reported for MOF/MXene photocatalysts, they are measured under monochromatic irradiation and remain modest: 4.25% at 350 nm dropping sharply to 0.19% at 400 nm for Cu_2[CuTCPP]/Ti_3C_2[60], and 3.14% at 420 nm for Ti_3C_2@MIL-NH_2[166]; the other cited systems do not report quantum efficiency. These values—especially the steep fall-off toward the visible range—remain well below the 10% solar-to-hydrogen conversion efficiency regarded as the minimum for competitively priced, large-scale photoelectrochemical systems[169].

Beyond hydrogen evolution, MOF/MXene hybrids exhibit photocatalytic performance spanning CO_2 photoreduction, ambient nitrogen fixation, and photocatalytic uranium(VI) reduction. For CO_2 conversion, *in situ* grown Co-Co LDH/Ti_3C_2 nanoarrays derived from MOF precursors deliver a CO generation rate of 1.25×10^4 μmol h^{-1} g^{-1} with an AQY of 0.92%[170]. Zn/Fe-ZIF/$Ti_3C_2T_x$ composites realize 96% epichlorohydrin conversion under simulated sunlight via photo-thermal synergism and extended near-infrared light response[59]. MXene quantum dot/Ni-MOF Type-II heterostructures activate N≡N triple bonds, attaining an ammonia production rate of 88.79 μmol g^{-1} h^{-1} under ambient light irradiation[171]. Similarly, MnO_x/UiO-66/Ti_3C_2 dual-cocatalyst systems realize 98.4% U(VI) photoreduction for radioactive wastewater treatment, extending the same interfacial design principles to actinide removal[172]. While these metrics appear promising, it is important to note that most photocatalytic tests are conducted in small-batch reactors under idealized conditions (pure water, controlled pH, sacrificial reagents for H_2 evolution). The

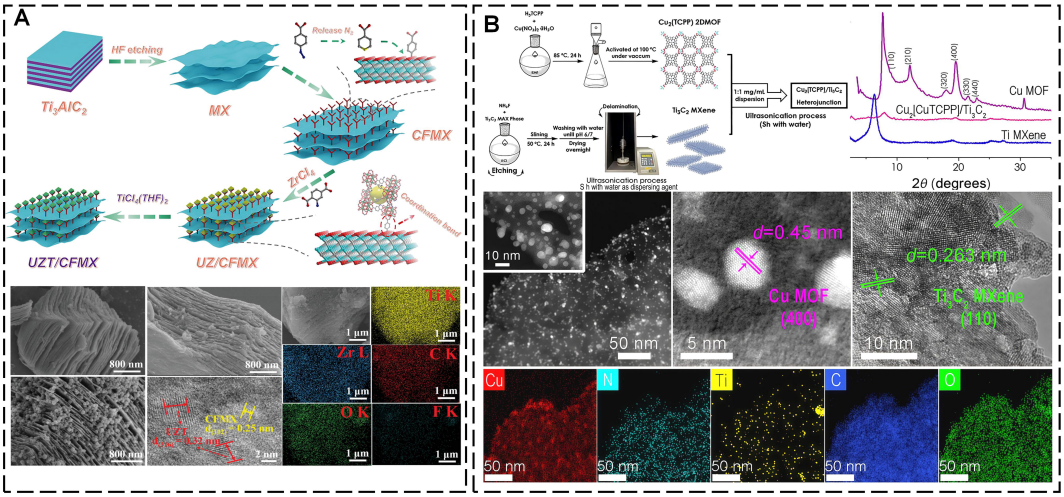


Figure 10. Synthesis strategies of MOF/MXene composites for photocatalysis. (A) Carboxyl group-assisted coordination route for constructing UiO-66-NH_2(Zr/Ti)/carboxyl-functionalized MXene (UZT/CFMX) heterostructure. Adapted from Ref.[61], under CC BY 4.0 license. (B) Assembly of 2D Cu_2[CuTCPP] MOF with exfoliated Ti_3C_2 MXene to form a 2D/2D Schottky junction for photocatalytic hydrogen evolution. Adapted from Ref.[60], under CC BY 4.0 license.

performance under realistic solar illumination and continuous-flow conditions is rarely reported, and the scalability of photocatalytic reactor design remains unexplored.

CONCLUSIONS AND FORECAST

Combining MOFs with MXenes is a strategy to develop heterostructured materials for energy applications. This design overcomes the inherent defects of single-component materials and integrates the advantages of both sides: MOFs offer high surface area, tunable porosity, and abundant redox-active sites, while MXenes provide metallic conductivity, mechanical flexibility, and unique surface chemistry. Interfacial chemical bonds such as Ti-O-Co form electron transport pathways. MXene skeletons stabilize active materials against structural damage, and diverse architectures from 0D/2D to 3D hierarchical networks optimize ion/electron transport. These advances enable MOF/MXene composites to achieve performance improvements in rechargeable batteries, supercapacitors, electrocatalysis, sensing, and photocatalysis.

Despite substantial progress, multiple challenges still hinder practical application. MXenes are prone to oxidation under electrochemical and thermal conditions, which degrades their conductivity and mechanical integrity over long-term operation. Current synthesis methods also face difficulties in large-scale production: MXene fabrication relies on hazardous fluoride-containing etchants, and MOF growth usually requires complex solvothermal conditions, raising concerns about environmental friendliness and production cost. It is also hard to guarantee batch consistency in mass production and achieve precise long-term interfacial regulation. In addition, MOF-derived components may undergo structural evolution during cycling, including interfacial delamination caused by volume expansion and gradual dissolution of metal active species. The lack of standardized testing protocols-particularly the near-universal reliance on low mass loadings, small electrolyte volumes, and short testing durations-means that laboratory performance metrics often overestimate practical viability. Further mechanism research is required to guide the design of more stable structures, and the field would benefit from greater transparency in reporting negative or null results.

The high cost of MOF/MXene composites originates mainly from expensive linkers (e.g., porphyrins, hexahydroxytriphenylene), non-earth-abundant metal nodes, and the multi-step HF-based MXene process. Several practical routes can reduce costs: use earth-abundant metals (Fe, Mn, Cu, Zn, Al) with cheap

commodity linkers such as terephthalic acid, 2-methylimidazole, and biomass-derived carboxylates; replace solvothermal batch synthesis with aqueous, room-temperature, or mechanochemical routes; develop fluoride-free MXene etching based on alkali-assisted, electrochemical, or eutectic-molten-salt routes; minimize the MXene content through 2D/2D designs in which a small amount of MXene forms a continuous conductive skeleton; and adopt continuous-flow, spray, or roll-to-roll processing. Life-cycle and techno-economic assessment should accompany these efforts to verify that the performance gain justifies the remaining cost premium.

To promote the industrial transformation of MOF/MXene composites from laboratory research, future studies can focus on the following directions. First, artificial intelligence and machine learning can be adopted for high-throughput screening and rational design of composite systems, to predict interfacial electronic structures and electrochemical performance before experimental verification. Second, developing fluoride-free green synthesis routes for MXenes and eco-friendly MOF fabrication methods such as mechanochemical synthesis and aqueous reaction will improve sustainability and scalability. Third, advanced structural engineering, including single-atom site design, Janus asymmetric interface construction, and 3D printing for customized devices, can unlock new functional properties. Finally, more research should focus on full-cell performance, long-term durability under practical working conditions (including high mass loadings, large-format cells, and continuous operation for > 1,000 h), and the development of flexible multifunctional devices. Interdisciplinary cooperation among materials scientists, electrochemical engineers, and manufacturing technologists will help MOF/MXene composites play a role in the global energy field.

DECLARATIONS

Acknowledgment

The components of the Graphical Abstract are reproduced from different sources under the CC BY 4.0 license: the "Batteries" diagram is from Ref.[63]; the "Electrochemical Catalysis" diagram is from Ref.[64]; the "Supercapacitors" diagram is from Ref.[65]; the "Sensing" diagram is from Ref.[66]; and the "Photochemical Catalysis" diagram is from Ref.[61].

Authors' contributions

Conceptualization, supervision, writing—review & editing, funding acquisition: Xu, B.
Investigation, writing—original draft: Sun, M.
Investigation, data curation: Li, Z.
Investigation: Ma, J.; Zhao, F.; Wang, X.
Supervision, resources, funding acquisition: Sun, D.
All authors have read and agreed to the published version of the manuscript.

Availability of data and materials

Not applicable.

AI and AI-assisted tools statement

Not applicable.

Financial support and sponsorship

This work was supported by the National Natural Science Foundation of China (Grant Nos. 22001265, 22275210, 22422112, 22371296), Natural Science Foundation of Shandong Province (Grant No. ZR2026MS0168), the Shandong Taishan Scholar Young Expert Project (No. tsqn202306126), Innovation fund project for graduate student of China University of Petroleum (East China), supported by "the Fundamental Research Funds for the Central Universities" (No. 26CX04032A), and the College Students' Innovative Entrepreneurial Training Plan Program (No. 202506014CX).

Conflicts of interest

All authors declared that there are no conflicts of interest.

Ethical approval and consent to participate

Not applicable.

Consent for publication

Not applicable.

Copyright

© The Author(s) 2026.

REFERENCES

1. Venkateswarlu, S.; Vallem, S.; Umer, M.; et al. Recent progress on MOF/MXene nanoarchitectures: a new era in coordination chemistry for energy storage and conversion. *J. Energy. Chem.* **2023**, *86*, 409-36. DOI
2. Cao, P.; Liu, Y.; Zhang, Q.; Guo, C.; Li, J.; Zeng, Q. MXene/MOF composites: synergistic platforms for advanced energy, catalysis, and environmental applications. *Coord. Chem. Rev.* **2025**, *545*, 217018. DOI
3. Gaba, L.; Siwach, P.; Aggarwal, K.; et al. Hybridization of metal-organic frameworks and MXenes: expanding horizons in supercapacitor applications. *Adv. Colloid. Interface. Sci.* **2024**, *332*, 103268. DOI
4. Chen, C.; Shen, L.; Wang, B.; et al. Environmental applications of metal-organic framework-based three-dimensional macrostructures: a review. *Chem. Soc. Rev.* **2025**, *54*, 2208-45. DOI
5. Kumar, S.; Jain, S.; Nehra, M.; Dilbaghi, N.; Marrazza, G.; Kim, K. Green synthesis of metal-organic frameworks: a state-of-the-art review of potential environmental and medical applications. *Coord. Chem. Rev.* **2020**, *420*, 213407. DOI
6. Shi, Y.; Yang, Y.; Ge, S.; et al. Progress in advanced MOF-derived materials for the removal of organic and inorganic pollutants. *Coord. Chem. Rev.* **2025**, *530*, 216474. DOI
7. Momtaz, E.; Amoozadeh, M.; Zarepour, A.; Khosravi, A.; Zarrabi, A.; Iravani, S. MXenes and MOFs for electrochemical reduction of carbon dioxide (CO_2). *RSC. Sustain.* **2026**, *4*, 1731-59. DOI
8. Hanan, A.; Lakhan, M. N.; Bibi, F.; et al. MOFs coupled transition metals, graphene, and MXenes: emerging electrocatalysts for hydrogen evolution reaction. *Chem. Eng. J.* **2024**, *482*, 148776. DOI
9. Ullah, S.; Qin, Z.; Tariq, M.; et al. MOF/MXene composite for electrocatalysis: fundamentals, structure-activity relationship and energy conversion applications. *Coord. Chem. Rev.* **2026**, *563*, 218037. DOI
10. Tahir, B.; Alraeesi, A.; Tahir, M. Metal-organic framework (MOF) integrated Ti_3C_2 MXene composites for CO_2 reduction and hydrogen production applications: a review on recent advances and future perspectives. *Front. Chem.* **2024**, *12*, 1448700. DOI PubMed PMC
11. Bagyalakshmi, S.; Balamurugan, K.; Mathankumar, M.; Sivakami, A.; Devi, N. Exploring metal organic frameworks/MXene based composite for an environmental applications-A critical review. *J. Mol. Struct.* **2025**, *1334*, 141838. DOI
12. Gopalakrishnan, M.; Kao-Ian, W.; Aupama, V.; et al. Metal-organic framework/mxene heterostructure and its derivatives as electrode materials for rechargeable Zn-based batteries: design strategies and perspectives. *Chem. Eng. J.* **2024**, *484*, 149624. DOI
13. Guo, H.; Zhang, J.; Xu, M.; et al. Zeolite-imidazole framework derived nickel-cobalt hydroxide on ultrathin MXene nanosheets for long life and high performance supercapacitance. *J. Alloys. Compd.* **2021**, *888*, 161250. DOI
14. Xiao, T.; Jin, J.; Zhang, Y.; et al. Rational construction of 2D/2D $Ti_3C_2T_x$/NiCo MOF heterostructure for highly efficient Li^+ storage. *Electrochim. Acta.* **2022**, *427*, 140851. DOI
15. Zheng, S.; Zhou, H.; Xue, H.; Braunstein, P.; Pang, H. Pillared-layer Ni-MOF nanosheets anchored on Ti_3C_2 MXene for enhanced electrochemical energy storage. *J. Colloid. Interface. Sci.* **2022**, *614*, 130-7. DOI PubMed
16. Li, Q.; Jiao, Q.; Yan, Y.; et al. Optimized Co-S bonds energy and confinement effect of hollow MXene@CoS_2/NC for enhanced sodium storage kinetics and stability. *Chem. Eng. J.* **2022**, *450*, 137922. DOI
17. Feng, L.; Chen, J.; Li, Y.; et al. MXene-reinforced Sb@C nanocomposites with synergizing spatial confinement architecture enabled ultra-stable and fast lithium ion storage. *Chem. Eng. J.* **2024**, *489*, 151396. DOI
18. Zhu, R.; Gu, Y.; Liu, L.; Lu, J.; Pang, H. Integration of conductive MOF and MXene for high-performance supercapacitor. *New. J. Chem.* **2024**, *48*, 10593-8. DOI
19. Wang, W.; Batool, N.; Zhang, T.; et al. When MOFs meet MXenes: superior ORR performance in both alkaline and acidic solutions. *J. Mater. Chem. A.* **2021**, *9*, 3952-60. DOI
20. Huang, T.; Huang, X.; Hu, C.; et al. MOF-derived Ni nanoparticles dispersed on monolayer MXene as catalyst for improved hydrogen storage kinetics of MgH. *Chem. Eng. J.* **2021**, *421*, 127851. DOI
21. Xu, B.; Wang, X.; Li, Z.; Zhao, F.; Sun, D. Recent progress in the in-situ growth of metal-organic frameworks on carbon-based supports. *Sci. China. Chem.* **2026**, *69*, 2735-52. DOI

22. Xu, B.; Zhao, F.; Li, Z.; et al. Regulated $Ni_3(HHTP)_2$ conjugated MOF nanorod array on GO support for elevated glucose sensing. *Chem. Eng. J.* **2026**, *530*, 173743. DOI
23. Zong, H.; Qi, R.; Yu, K.; Zhu, Z. Ultrathin Ti_2NT_x MXene-wrapped MOF-derived CoP frameworks towards hydrogen evolution and water oxidation. *Electrochim. Acta.* **2021**, *393*, 139068. DOI
24. Murtaza, M.; Farooq, K.; Shah, W. A.; Ahmad, I.; Waseem, A. Layered MOF supported on 2D delaminated MXene ($Mo_2Ti_2C_3$) nanosheets boosted water splitting. *Nanoscale. Adv.* **2024**, *6*, 6317-27. DOI PubMed PMC
25. Lamiel, C.; Hussain, I.; Warner, J. H.; Zhang, K. Beyond Ti-based MXenes: a review of emerging non-Ti based metal-MXene structure, properties, and applications. *Mater. Today.* **2023**, *63*, 313-38. DOI
26. Jiang, Q.; Lei, Y.; Liang, H.; Xi, K.; Xia, C.; Alshareef, H. N. Review of MXene electrochemical microsupercapacitors. *Energy. Storage. Mater.* **2020**, *27*, 78-95. DOI
27. Oh, T.; Lee, S.; Kim, H.; Ko, T. Y.; Kim, S. J.; Koo, C. M. Fast and high-yield anhydrous synthesis of $Ti_3C_2T_x$ MXene with high electrical conductivity and exceptional mechanical strength. *Small* **2022**, *18*, 2203767. DOI
28. Lipatov, A.; Goad, A.; Loes, M. J.; et al. High electrical conductivity and breakdown current density of individual monolayer Ti_3C_2T MXene flakes. *Matter* **2021**, *4*, 1413-27. DOI
29. Lipatov, A.; Bagheri, S.; Sinitskii, A. Metallic conductivity of $Ti_3C_2T_x$ MXene confirmed by temperature-dependent electrical measurements. *ACS. Mater. Lett.* **2023**, *6*, 298-307. DOI
30. Loes, M. J.; Bagheri, S.; Sinitskii, A. Layer-dependent gas sensing mechanism of 2D titanium carbide ($Ti_3C_2T_x$) MXene. *ACS. Nano.* **2024**, acsnano.4c08225. DOI PubMed
31. Kenaz, R.; Ghosh, S.; Lounasvuori, M.; et al. Optical, structural, and charge transport properties of individual $Ti_3C_2T_x$ MXene flakes via micro-ellipsometry and beyond. *ACS. Nano.* **2025**, *19*, 35414-24. DOI
32. Yang, X.; Xu, C.; Li, S.; et al. Thermal treatment for promoting interfacial interaction in Co-BDC/Ti_3C_2T hybrid nanosheets for hybrid supercapacitors. *J. Colloid. Interface. Sci.* **2022**, *617*, 633-40. DOI
33. Zhao, L.; Dong, B.; Li, S.; et al. Interdiffusion reaction-assisted hybridization of two-dimensional metal-organic frameworks and $Ti_3C_2T_x$ nanosheets for electrocatalytic oxygen evolution. *ACS. Nano.* **2017**, *11*, 5800-7. DOI
34. Yang, X.; Tian, Y.; Li, S.; et al. Heterogeneous Ni-MOF/V_2CT_x-MXene hierarchically-porous nanorods for robust and high energy density hybrid supercapacitors. *J. Mater. Chem. A.* **2022**, *10*, 12225-34. DOI
35. Saini, H.; Srinivasan, N.; Šedajová, V.; et al. Emerging MXene@metal-organic framework hybrids: design strategies toward versatile applications. *ACS. Nano.* **2021**, *15*, 18742-76. DOI
36. Prabhakar Vattikuti, S. V.; Shim, J.; Rosaiah, P.; Mauger, A.; Julien, C. M. Recent advances and strategies in MXene-based electrodes for supercapacitors: applications, challenges and future prospects. *Nanomaterials* **2023**, *14*, 62. DOI PubMed PMC
37. Chen, Y.; Shi, Y.; Song, G.; Yang, B.; Pang, H. Compositing MXene with organic coordination frameworks (MOFs, COFs, and HOFs) for enhanced electrochemical performance. *Next. Mater.* **2025**, *6*, 100323. DOI
38. Singha, A.; Pandey, P.; Sahu, A.; Qureshi, M. Ultrathin dielectric triggered charge injection dynamics for high-performance metal organic framework/MXene supercapacitors. *J. Phys. Chem. Lett.* **2024**, *15*, 2123-32. DOI PubMed
39. Wu, G.; Sun, S.; Zhu, X.; Ma, Z.; Zhang, Y.; Bao, N. Microfluidic fabrication of hierarchical-ordered ZIF-L(Zn)@ $Ti_3C_2T_x$ Core-sheath fibers for high-performance asymmetric supercapacitors. *Angew. Chem. Int. Ed.* **2021**, *61*, e202115559. DOI
40. Xu, D.; Zhang, Z.; Tao, K.; Han, L. A heterostructure of a 2D bimetallic metal-organic framework assembled on an MXene for high-performance supercapacitors. *Dalton. Trans.* **2023**, *52*, 2455-62. DOI
41. Fang, T.; Ma, J.; Dai, Y.; et al. 2D sandwich-like Co-MOF/MXene composites as self-reconstructive oxygen evolution electrocatalysts. *ACS. Appl. Nano. Mater.* **2025**, *8*, 3519-26. DOI
42. Watwiangkham, A.; Zijdemans, P. A.; Hadsadee, S.; et al. Rational design of MXene/MOF heterostructures to suppress hydrogen evolution and mitigate dendrite growth in aqueous Zn-ion batteries: insights from DFT and MD studies. *ACS. Appl. Mater. Interfaces.* **2025**, *17*, 69245-56. DOI
43. Yang, Z.; Weng, C.; Gao, X.; et al. In situ construction of Sn-based metal-organic frameworks on MXene achieving fast electron transfer for rapid lithium storage. *Chem. Eng. J.* **2024**, *486*, 150299. DOI
44. Zhang, P.; Chen, J.; Feng, L.; Jiang, M.; Xu, B. Dual confinement of Si nanoparticles in a MXene/ZIF-8-derived carbon framework for lithium-ion batteries. *ACS. Appl. Nano. Mater.* **2022**, *5*, 12720-8. DOI
45. Hu, R.; Sha, D.; Cao, X.; et al. Anchoring metal-organic framework-derived ZnTe@C onto elastic $Ti_3C_2T_x$ MXene with 0D/2D dual confinement for ultrastable potassium-ion storage. *Adv. Energy. Mater.* **2022**, *12*, 2203118. DOI
46. Liu, Y.; Shi, Z.; Liang, T.; et al. The mechanism of room-temperature oxidation of aHF-etched $Ti_3C_2T_x$ MXene determined via environmental transmission electron microscopy and molecular dynamics. *InfoMat* **2024**, *6*, e12536. DOI

47. Soomro, R. A.; Zhang, P.; Fan, B.; Wei, Y.; Xu, B. Progression in the oxidation stability of MXenes. *Nano-Micro. Lett.* **2023**, *15*, 108. DOI PubMed PMC
48. Chen, Y.; Cheng, J.; Wang, A.; et al. The enhanced performance of Li-ion batteries based on Co-MOF/MXene composites. *Inorg. Chem. Commun.* **2024**, *159*, 111793. DOI
49. Gao, X.; Zheng, Y.; Chang, J.; et al. Universal strategy for preparing highly stable PBA/$Ti_3C_2T_x$ MXene toward lithium-ion batteries *via* chemical transformation. *ACS. Appl. Mater. Interfaces.* **2022**, *14*, 15298-306. DOI
50. Sun, L.; Sun, J.; Zhai, S.; et al. Homologous MXene-derived electrodes for potassium-ion full batteries. *Adv. Energy. Mater.* **2022**, *12*, 2200113. DOI
51. Chen, X.; Wang, K.; Xie, K.; Tao, H.; Wang, Y. MXene-coated nickel ion-exchanged ZIF skeleton-cavity layered double hydroxides for supercapacitors. *Energy. Fuels.* **2022**, *37*, 763-73. DOI
52. Zhang, X.; Yang, S.; Lu, W.; et al. MXenes induced formation of Ni-MOF microbelts for high-performance supercapacitors. *J. Colloid. Interface. Sci.* **2021**, *592*, 95-102. DOI
53. Tamtam, M. R.; Vangala, S. P. K.; Subrahmanyeswara Rao, N.; Choi, G. S.; Shim, J. MXene-coupled Mn-V binary MOF: a dual approach to stability enhancement and capacitance amplification. *Ceram. Int.* **2026**, *52*, 15876-88. DOI
54. Zhao, W.; Peng, J.; Wang, W.; et al. Interlayer hydrogen-bonded metal porphyrin frameworks/MXene hybrid film with high capacitance for flexible all-solid-state supercapacitors. *Small* **2019**, *15*, 1901351. DOI
55. Manikandan, M.; Seyadu Abuthahir, P.; Senthilkumar, P.; Manikandan, E. Synthesis of a MXene/metal-organic framework composite for efficient supercapacitor and electrocatalytic CO_2 reduction. *ACS. Appl. Mater. Interfaces.* **2025**, *17*, 51996-2009. DOI
56. Leng, X.; Vattikuti, S. P.; Zeng, J.; et al. Bimetallic Ni-Mo-MOFs as multifunctional electrodes for high-performance supercapacitors and oxygen evolution reaction. *Int. J. Hydrogen. Energy.* **2026**, *218*, 153954. DOI
57. Nazari, M.; Morsali, A. Trimetallic-organic framework/MXene composite as an oxygen evolution reaction electrocatalyst with elevated intrinsic activity. *J. Mater. Chem. A.* **2024**, *12*, 4826-34. DOI
58. Xie, Y.; Liu, G.; Rao, Z.; et al. In situ growth of CoFe bimetallic MOFs on S-Mxene/NF composite substrate as an efficient electrocatalyst for OER. *Energy. Fuels.* **2025**, *39*, 23304-13. DOI
59. Wang, Y.; Ding, M.; Rong, W.; Kong, S.; Yao, J. In situ growth of Fe-doped zeolitic imidazolate framework on MXene for boosting photodriven CO_2 cycloaddition. *Sep. Purif. Technol.* **2024**, *345*, 127399. DOI
60. Cabrero-Antonino, M.; Uscategui-Linares, A.; Ramírez-Grau, R.; et al. 2D/2D MOF/MXene schottky junction: prolonged carrier lifetime and enhanced hydrogen evolution efficiency. *Angew. Chem. Int. Ed.* **2025**, *64*, e202503860. DOI
61. Shi, L.; Wu, C.; Wang, Y.; et al. Rational design of coordination bond connected metal organic frameworks/MXene hybrids for efficient solar water splitting. *Adv. Funct. Mater.* **2022**, *32*, 2202571. DOI
62. Cao, B.; Liu, H.; Zhang, X.; et al. MOF-derived ZnS nanodots/$Ti_3C_2T_x$ MXene hybrids boosting superior lithium storage performance. *Nano. Micro. Lett.* **2021**, *13*, 202. DOI PubMed PMC
63. Chen, A.; Wang, J.; Chen, L.; et al. Hydroxylated MXene-assisted in situ synthesis of ultrafine CoHCC nanoparticles for high-performance potassium-ion battery anodes. *Energy. . Environ. Mater.* **2026**, e70447. DOI
64. Yu, K.; Zhang, J.; Hu, Y.; Wang, L.; Zhang, X.; Zhao, B. Ni doped Co-MOF-74 synergized with 2D $Ti_3C_2T_x$ MXene as an efficient electrocatalyst for overall water-splitting. *Catalysts* **2024**, *14*, 184. DOI
65. Liu, Y.; Pan, M.; Gong, M.; et al. Boosting redox kinetics in CoS/Ti_3C_2 heterostructure via interfacial charge redistribution for high-energy-density supercapacitors. *Green. Energy. Environ.* **2026**, *11*, 464-77. DOI
66. Zhang, H.; Cao, W.; Wang, J.; et al. 2D conductive MOFs intercalated in MXene interlayer for fast and trace detection of triethylamine at room temperature. *Adv. Sci.* **2025**, *12*, 2500786. DOI PubMed PMC
67. Adil, M.; Olabi, A. G.; Abdelkareem, M. A.; et al. In-situ grown metal-organic framework derived CoS-MXene pseudocapacitive asymmetric supercapacitors. *J. Energy. Storage.* **2023**, *60*, 106537. DOI
68. Jiang, G.; Zheng, N.; Chen, X.; et al. In-situ decoration of MOF-derived carbon on nitrogen-doped ultrathin MXene nanosheets to multifunctionalize separators for stable Li-S batteries. *Chem. Eng. J.* **2019**, *373*, 1309-18. DOI
69. Yu, T.; Li, S.; Zhang, L.; et al. In situ growth of ZIF-67-derived nickel-cobalt-manganese hydroxides on 2D V_2CT_x MXene for dual-functional orientation as high-performance asymmetric supercapacitor and electrochemical hydroquinone sensor. *J. Colloid. Interface. Sci.* **2023**, *629*, 546-58. DOI
70. Li, P.; Chong, X.; Guo, Y.; et al. Heterostructure-engineered conductive MOFs coupled with $MoSe_2$@MXene framework for efficient and selective lithium extraction from salt lake brine via capacitive deionization. *Adv. Sci.* **2026**, *13*, e21830. DOI PubMed PMC
71. Ji, Y.; Li, W.; You, Y.; Xu, G. In situ synthesis of M (Fe, Cu, Co and Ni)-MOF@MXene composites for enhanced specific capacitance and cyclic stability in supercapacitor electrodes. *Chem. Eng. J.* **2024**, *496*, 154009. DOI

72. Liu, J.; Xia, Q.; Wang, L.; Hu, Q.; Shinde, N. M.; Zhou, A. In situ growth of nanorod-shaped Ni_3Co-MOF on Mo_2CT_x MXene surface to realize enhanced energy storage for supercapacitors. *ACS. Appl. Mater. Interfaces.* **2024**, *16*, 49380-91. DOI
73. Wei, J.; Hu, F.; Pan, Y.; Lv, C.; Bian, L.; Ouyang, Q. Design strategy for metal-organic framework assembled on modifications of MXene layers for advanced supercapacitor electrodes. *Chem. Eng. J.* **2024**, *481*, 148793. DOI
74. Yue, L.; Chen, L.; Wang, X.; et al. Ni/Co-MOF@aminated MXene hierarchical electrodes for high-stability supercapacitors. *Chem. Eng. J.* **2023**, *451*, 138687. DOI
75. Stock, N.; Biswas, S. Synthesis of metal-organic frameworks (MOFs): routes to various MOF topologies, morphologies, and composites. *Chem. Rev.* **2011**, *112*, 933-69. DOI PubMed
76. Meng, Y.; Yue, F.; Zhang, S.; et al. Zr-MOF/MXene composite for enhanced photothermal catalytic CO_2 reduction in atmospheric and industrial flue gas streams. *Carbon. Capture. Sci. Technol.* **2024**, *13*, 100274. DOI
77. Ren, Y.; Zhai, Q.; Wang, B.; et al. Synergistic adsorption-electrocatalysis of 2D/2D heterostructure toward high performance Li-S batteries. *Chem. Eng. J.* **2022**, *439*, 135535. DOI
78. Huang, P.; Ying, H.; Zhang, S.; Zhang, Z.; Han, W. Multidimensional synergistic architecture of Ti_3C_2 MXene/CoS_2@N-doped carbon for sodium-ion batteries with ultralong cycle lifespan. *Chem. Eng. J.* **2022**, *429*, 132396. DOI
79. Wu, W.; Liu, T.; Diwu, J.; Li, C.; Zhu, J. Metal-organic framework-derived $NiCo_2S_4$@Co_3S_4 yolk-shell nanocages/ $Ti_3C_2T_x$ MXene for high-performance asymmetric supercapacitors. *J. Alloys. Compd.* **2023**, *954*, 170213. DOI
80. Tan, P.; Gao, R.; Zhang, Y.; et al. Electrostatically directed assembly of two-dimensional ultrathin Co_2Ni-MOF/$Ti_3C_2T_x$ nanosheets for electrocatalytic oxygen evolution. *J. Colloid. Interface. Sci.* **2023**, *630*, 363-71. DOI
81. Qi, J. Q.; Huang, M. Y.; Ruan, C. Y.; et al. Construction of $CoNi_2S_4$ nanocubes interlinked by few-layer $Ti_3C_2T_x$ MXene with high performance for asymmetric supercapacitors. *Rare. Metals.* **2022**, *41*, 4116-26. DOI
82. Xie, W.; Wang, Y.; Zhou, J.; et al. MOF-derived $CoFe_2O_4$ nanorods anchored in MXene nanosheets for all pseudocapacitive flexible supercapacitors with superior energy storage. *Appl. Surf. Sci.* **2020**, *534*, 147584. DOI
83. Guo, H.; Zhang, J.; Yang, F.; et al. Sandwich-like porous MXene/Ni_3S_4/CuS derived from MOFs as superior supercapacitor electrode. *J. Alloys. Compd.* **2022**, *906*, 163863. DOI
84. Zhang, H.; Li, Z.; Hou, Z.; et al. Self-assembly of MOF on MXene nanosheets and in-situ conversion into superior nickel phosphates/MXene battery-type electrode. *Chem. Eng. J.* **2021**, *425*, 130602. DOI
85. Zou, H.; He, B.; Kuang, P.; Yu, J.; Fan, K. Metal-organic framework-derived nickel-cobalt sulfide on ultrathin Mxene nanosheets for electrocatalytic oxygen evolution. *ACS. Appl. Mater. Interfaces.* **2018**, *10*, 22311-9. DOI
86. Zong, H.; Hu, L.; Wang, Z.; Qi, R.; Yu, K.; Zhu, Z. Metal-organic frameworks-derived CoP anchored on MXene toward an efficient bifunctional electrode with enhanced lithium storage. *Chem. Eng. J.* **2021**, *416*, 129102. DOI
87. Liu, X.; Liu, Z.; Yang, W.; et al. In situ fragmented and confined CoP nanocrystals into sandwich-structure MXene@CoP@NPC heterostructure for superior sodium-ion storage. *Mater. Today. Chem.* **2022**, *26*, 101002. DOI
88. Liu, X.; Liu, F.; Zhao, X.; Fan, L. Constructing MOF-derived CoP-NC@MXene sandwich-like composite by in-situ intercalation for enhanced lithium and sodium storage. *J. Materiomics.* **2022**, *8*, 30-7. DOI
89. Murtaza, M.; Farooq, K.; Shah, W. A.; Waseem, A. CoBDC MOF derived CoP/C couple with 2D Nb_2CT_x MXene as an efficient bifunctional catalyst for water splitting. *Fuel* **2025**, *394*, 135095. DOI
90. Farooq, K.; Yang, Z.; Murtaza, M.; et al. MXene-enhanced metal-organic framework-derived CoP nanocomposites as highly efficient trifunctional electrocatalysts for OER, HER, and ORR. *Adv. Energy. Sustain. Res.* **2025**, *6*, 2400400. DOI
91. Xiao, T.; Zhang, Y.; Xi, W.; et al. Rationally designing a $Ti_3C_2T_x$/CNTs-Co_9S_8 heterostructure as a sulfur host with multi-functionality for high-performance lithium-sulfur batteries. *Nanoscale* **2022**, *14*, 16139-47. DOI
92. Ruan, C.; Zhu, D.; Qi, J.; et al. MXene-modulated $CoNi_2S_4$ dendrite as enhanced electrode for hybrid supercapacitors. *Surf. Interfaces.* **2021**, *25*, 101274. DOI
93. Wen, Y.; Rufford, T. E.; Chen, X.; et al. Nitrogen-doped $Ti_3C_2T_x$ MXene electrodes for high-performance supercapacitors. *Nano. Energy.* **2017**, *38*, 368-76. DOI
94. Zhang, C.; Wang, L.; Lei, W.; et al. Achieving quick charge/discharge rate of 3.0 V s^{-1} by 2D titanium carbide (MXene) via N-doped carbon intercalation. *Mater. Lett.* **2019**, *234*, 21-5. DOI
95. Jiang, J.; Xi, C.; Zhao, Y.; et al. MXene-based hierarchical electron coupling engineering of F-doped NiFe LDH/MOF-74 electrocatalysts for efficient overall water splitting. *ACS. Catal.* **2025**, *15*, 2561-75. DOI
96. Niu, H.; Yan, Y.; Jiang, S.; et al. Interfaces decrease the alkaline hydrogen-evolution kinetics energy barrier on NiCoP/$Ti_3C_2T_x$ MXene. *ACS. Nano.* **2022**, *16*, 11049-58. DOI

97. Natu, V.; Benchakar, M.; Canaff, C.; Habrioux, A.; Célérier, S.; Barsoum, M. W. A critical analysis of the X-ray photoelectron spectra of $Ti_3C_2T_z$ MXenes. *Matter* **2021**, *4*, 1224-51. DOI
98. Wen, C.; Guo, D.; Zheng, X.; Li, H.; Sun, G. Hierarchical *n* MOF-867/MXene nanocomposite for chemical adsorption of polysulfides in lithium-sulfur batteries. *ACS. Appl. Energy. Mater.* **2021**, *4*, 8231-41. DOI
99. Wang, Y.; Song, J.; Wong, W. Y. Constructing 2D sandwich-like MOF/MXene heterostructures for durable and fast aqueous zinc-ion batteries. *Angew. Chem. Int. Ed.* **2023**, *62*, e202218343. DOI
100. Sun, K.; Shen, Y.; Min, J.; et al. MOF-derived Zn/Co co-doped MnO/C microspheres as cathode and Ti_3C_2@Zn as anode for aqueous zinc-ion full battery. *Chem. Eng. J.* **2023**, *454*, 140394. DOI
101. Kao, Y.; Young, C. Trimetallic oxide catalysts from metal-organic frameworks on $Ti_3C_2T_x$ MXene for enhanced water splitting. *Int. J. Hydrogen. Energy.* **2025**, *100*, 704-12. DOI
102. Liang, X.; Ren, X.; Yang, Q.; et al. A two-dimensional MXene-supported metal-organic framework for highly selective ambient electrocatalytic nitrogen reduction. *Nanoscale* **2021**, *13*, 2843-8. DOI
103. Liu, Z.; Lv, H.; Zhang, Y.; et al. Synergistic etching and hydrogen bonding-induced self-assembly of MXene/MOF hybrid aerogel for flexible room-temperature gas sensing. *ACS. Sens.* **2024**, *9*, 3641-51. DOI
104. Chang, Y.; Chen, M.; Fu, Z.; et al. Building porphyrin-based MOFs on MXenes for ppb-level NO sensing. *J. Mater. Chem. A.* **2023**, *11*, 6966-77. DOI
105. Liu, Y.; He, Y.; Vargun, E.; Plachy, T.; Saha, P.; Cheng, Q. 3D porous Ti_3C_2 MXene/NiCo-MOF composites for enhanced lithium storage. *Nanomaterials* **2020**, *10*, 695. DOI PubMed PMC
106. He, J.; Wei, Y.; Zhai, T.; Li, H. Antimony-based materials as promising anodes for rechargeable lithium-ion and sodium-ion batteries. *Mater. Chem. Front.* **2018**, *2*, 437-55. DOI
107. Liang, S.; Cheng, Y. J.; Zhu, J.; Xia, Y.; Müller-Buschbaum, P. A chronicle review of nonsilicon (Sn, Sb, Ge)-based lithium/sodium-ion battery alloying anodes. *Small. Methods.* **2020**, *4*, 2000218. DOI
108. Sun, L.; Wang, H.; Zhai, S.; et al. Dual-conductive metal-organic framework@MXene heterogeneity stabilizes lithium-ion storage. *J. Energy. Chem.* **2023**, *76*, 368-76. DOI
109. Hwang, J.; Myung, S.; Sun, Y. Sodium-ion batteries: present and future. *Chem. Soc. Rev.* **2017**, *46*, 3529-614. DOI
110. Xu, E.; Li, P.; Quan, J.; et al. Dimensional gradient structure of $CoSe_2$@CNTs-MXene anode assisted by ether for high-capacity, stable sodium storage. *Nano. Micro. Lett.* **2021**, *13*, 40. DOI PubMed PMC
111. Wang, T.; Zeng, J.; Gu, X.; et al. In-situ growth of nitrogen-doped carbon nanotubes on MXene nanosheets for efficient sodium/potassium-ion storage. *Front. Mater.* **2023**, *10*, 1214543. DOI
112. Shi, X.; Liang, W.; Liu, G.; et al. Electrode materials for Li/Na storage from mechanochemically synthesised MOFs/MXene composites: a solvent-free approach. *Chem. Eng. J.* **2023**, *462*, 142271. DOI
113. Li, Y.; Wu, F.; Li, Y.; et al. Ether-based electrolytes for sodium ion batteries. *Chem. Soc. Rev.* **2022**, *51*, 4484-536. DOI
114. Mane, R. S.; Mane, S.; Somkuwar, V.; Thombre, N. V.; Patwardhan, A. V.; Jha, N. A novel hierarchically hybrid structure of MXene and bi-ligand ZIF-67 based trifunctional electrocatalyst for zinc-air battery and water splitting. *Battery. Energy.* **2023**, *2*, 20230019. DOI
115. Lu, H.; Hu, J.; Zhang, K.; et al. Microfluidic-assisted 3D printing zinc powder anode with 2D conductive MOF/MXene heterostructures for high-stable zinc-organic battery. *Adv. Mater.* **2023**, *36*, 2309753. DOI
116. Ahmed, A. A.; Mirghni, A. A.; Hardianto, Y. P.; et al. Engineering a hierarchically porous manganese-based ternary composite for high-performance aqueous zinc-ion batteries. *J. Inorg. Organomet. Polym. Mater.* **2026**, 4344. DOI
117. Hosaka, T.; Kubota, K.; Hameed, A. S.; Komaba, S. Research development on K-ion batteries. *Chem. Rev.* **2020**, *120*, 6358-466. DOI PubMed
118. Pathak, I.; Acharya, D.; Chhetri, K.; et al. $Ti_3C_2T_x$ MXene integrated hollow carbon nanofibers with polypyrrole layers for MOF-derived freestanding electrodes of flexible asymmetric supercapacitors. *Chem. Eng. J.* **2023**, *469*, 143388. DOI
119. Adil, M.; Olabi, A. G.; Abdelkareem, M. A.; et al. In-situ grown bimetallic FeCu MOF-MXene composite for solid-state asymmetric supercapacitors. *J. Energy. Storage.* **2023**, *68*, 107817. DOI
120. Liu, C.; Bai, Y.; Li, W.; Yang, F.; Zhang, G.; Pang, H. In situ growth of three-dimensional MXene/metal-organic framework composites for high-performance supercapacitors. *Angew. Chem. Int. Ed.* **2022**, *61*, e202116282. DOI
121. Dai, Y.; Sun, C.; Gul, H.; et al. Three-dimensional honeycomb composites consist of metal carbides and layered double hydroxides for high-performance supercapacitor electrode materials. *J. Power. Sources.* **2024**, *602*, 234306. DOI
122. Shivade, D. S.; Kurade, A. N.; Bhosale, R. K.; et al. Folic acid-assisted in situ solvothermal synthesis of Ni-MOF/MXene composite for high-performance supercapacitors. *J. Energy. Storage.* **2024**, *100*, 113754. DOI
123. Adil, M.; Olabi, A. G.; Abdelkareem, M. A.; Alawadhi, H.; Shinde, P. A.; Rodriguez, C. Engineering MXene-Fe MOF interfaces through in-situ growth for high-performance hybrid supercapacitors. *J. Power. Sources.* **2026**, *666*, 239129. DOI

124. Han, Y.; Liu, Z.; Wang, C.; Guo, L.; Wang, Y. Construction of rod-like cobalt-pyridinedicarboxylic acid/MXene nanosheets composites for hydrogen evolution reaction and supercapacitor. *J. Colloid. Interface. Sci.* **2024**, *661*, 139-49. DOI
125. Wang, J.; Gong, J.; Zhang, H.; Lv, L.; Liu, Y.; Dai, Y. Construction of hexagonal nickel-cobalt oxide nanosheets on metal-organic frameworks based on MXene interlayer ion effect for hybrid supercapacitors. *J. Alloys. Compd.* **2021**, *870*, 159466. DOI
126. Du, Z.; Liu, W.; Liu, J.; et al. A thermally chargeable supercapacitor based on the g-C_3N_4-doped PAMPS/PAA hydrogel solid electrolyte and 2D MOF@$Ti_3C_2T_x$ MXene heterostructure composite electrode. *Adv. Mater. Inter.* **2023**, *10*, 2300266. DOI
127. Li, S.; Wang, Y.; Li, Y.; Xu, J.; Li, T.; Zhang, T. In situ growth of Ni-MOF nanorods array on $Ti_3C_2T_x$ nanosheets for supercapacitive electrodes. *Nanomaterials* **2023**, *13*, 610. DOI PubMed PMC
128. Zhang, Y.; Zhu, X.; Sun, S.; Guo, Q.; Xu, M.; Wu, G. Ordered interface engineering enabled high-performance $Ti_3C_2T_x$ MXene fiber-based supercapacitors. *Energy. Fuels.* **2022**, *36*, 7898-907. DOI
129. Shingte, S.; Chavan, V.; Dhavale, R.; et al. Optimizing supercapacitive performance of MXene through MOF-derived nickel ferrite nanoparticle integration. *J. Energy. Storage.* **2024**, *92*, 112169. DOI
130. Maity, S.; Bera, S.; Kapuria, A.; Debnath, A.; Das, S.; Saha, S. K. MXene derived metal organic framework@PANI heterostructure as a hybrid supercapacitor. *Mater. Today. Chem.* **2025**, *45*, 102690. DOI
131. Tamtam, M. R.; Karri, R. R.; Choi, G. S.; Shim, J. MXene-integrated Mn Co bimetallic MOF hybrids for enhanced solid-state supercapacitor performance. *J. Energy. Storage.* **2026**, *154*, 120355. DOI
132. Movafagh, R.; Ghamari, F.; Shi, H.; Arjomandi, J. Template-assisted construction of NiCo-MOF/MXene nanocomposite based on poly p-nitroaniline as efficient electrode material for symmetric and asymmetric hybrid supercapacitors. *J. Energy. Storage.* **2026**, *141*, 119321. DOI
133. Gogotsi, Y.; Simon, P. True Performance Metrics in Electrochemical Energy Storage. *Science* **2011**, *334*, 917-8. DOI PubMed
134. Roger, I.; Shipman, M. A.; Symes, M. D. Earth-abundant catalysts for electrochemical and photoelectrochemical water splitting. *Nat. Rev. Chem.* **2017**, *1*, 0003. DOI
135. Gu, W.; Wu, M.; Xu, J.; Zhao, T. MXene boosted metal-organic framework-derived Fe-N-C as an efficient electrocatalyst for oxygen reduction reactions. *Int. J. Hydrogen. Energy.* **2022**, *47*, 17224-32. DOI
136. Zhang, J.; Zhang, W.; Zhang, J.; et al. MOF-derived bimetallic NiMo-based sulfide electrocatalysts for efficient hydrogen evolution reaction in alkaline media. *J. Alloys. Compd.* **2023**, *935*, 167974. DOI
137. Pashajavid, S.; Mohammadi, T.; Hanifi, S.; Asghari, E.; Delibaş, N.; Niaei, A. Boosted oxygen evolution with engineering of mixed ligand Co metal-organic framework integrated on titanium carbide MXene support. *Diamond. Relat. Mater.* **2026**, *166*, 113762. DOI
138. Farooq, K.; Murtaza, M.; Yang, Z.; Waseem, A.; Zhu, Y.; Xia, Y. MXene boosted MOF-derived cobalt sulfide/carbon nanocomposites as efficient bifunctional electrocatalysts for OER and HER. *Nanoscale. Adv.* **2024**, *6*, 3169-80. DOI PubMed PMC
139. Wen, Y.; Wei, Z.; Ma, C.; Xing, X.; Li, Z.; Luo, D. MXene boosted CoNi-ZIF-67 as highly efficient electrocatalysts for oxygen evolution. *Nanomaterials* **2019**, *9*, 775. DOI PubMed PMC
140. Tiwari, A. P.; Chandra, P.; Rahman, M. S.; Mirica, K. A.; Scheideler, W. J. Optimizing active sites*via* chemical bonding of 2D metal-organic frameworks and MXenes for efficient hydrogen evolution reaction activity. *Nanoscale* **2025**, *17*, 11028-36. DOI PubMed
141. Mirghni, A. A.; Hardianto, Y. P.; Ferdous, A. R.; Shah, S. S.; Hossain, M. D.; Aziz, M. A. Scalable electrodeposition of NiMoP for alkaline hydrogen production: from catalyst design to full-cell performance. *Electrochim. Acta.* **2026**, *572*, 149291. DOI
142. Li, S.; Chai, H.; Zhang, L.; Xu, Y.; Jiao, Y.; Chen, J. Constructing oxygen vacancy-rich MXene @Ce-MOF composites for enhanced energy storage and conversion. *J. Colloid. Interface. Sci.* **2023**, *642*, 235-45. DOI
143. Felgenhauer, M.; Hamacher, T. State-of-the-art of commercial electrolyzers and on-site hydrogen generation for logistic vehicles in South Carolina. *Int. J. Hydrogen. Energy.* **2015**, *40*, 2084-90. DOI
144. Buttler, A.; Spliethoff, H. Current status of water electrolysis for energy storage, grid balancing and sector coupling via power-to-gas and power-to-liquids: a review. *Renew. Sustain. Energy. Rev.* **2018**, *82*, 2440-54. DOI
145. He, L.; Liu, J.; Hu, B.; et al. Cobalt oxide doped with titanium dioxide and embedded with carbon nanotubes and graphene-like nanosheets for efficient trifunctional electrocatalyst of hydrogen evolution, oxygen reduction, and oxygen evolution reaction. *J. Power. Sources.* **2019**, *414*, 333-44. DOI
146. Huang, H.; Qin, J.; Liu, C.; et al. Constructing Zn-based MOF-MXene nanoarchitectures to stabilize ultrafine Pt nanocrystals with enhanced methanol oxidation performance. *Carbon* **2024**, *226*, 119171. DOI
147. Voiry, D.; Chhowalla, M.; Gogotsi, Y.; et al. Best practices for reporting electrocatalytic performance of nanomaterials. *ACS. Nano.* **2018**, *12*, 9635-8. DOI
148. Paul, J.; Kim, J. Reticular synthesis of a conductive composite derived from metal-organic framework and Mxene for the electrochemical detection of dopamine. *Appl. Surf. Sci.* **2023**, *613*, 156103. DOI

149. Rodrigues, P.; Bangali, H.; Saleh, E. A. M.; et al. Metal-organic framework/MXene nanohybrid composites as an emerging electrochemical sensing platform for food safety and biomedical monitoring: from synthesis to application. *Electrochim. Acta.* **2024**, *494*, 144424. DOI
150. Ramachandran, R.; Zhao, C.; Rajkumar, M.; et al. Porous nickel oxide microsphere and $Ti_3C_2T_x$ hybrid derived from metal-organic framework for battery-type supercapacitor electrode and non-enzymatic H_2O_2 sensor. *Electrochim. Acta.* **2019**, *322*, 134771. DOI
151. Peng, H.; Yang, J.; Lin, C.; Qi, L.; Li, L.; Shi, K. Gas-sensitive performance of metal-organic framework-derived CuO NPs/$Ti_3C_2T_x$ MXene heterostructures for efficient NO_2 detection at room temperature. *J. Alloys. Compd.* **2024**, *980*, 173657. DOI
152. Ranjith, K. S.; Sonwal, S.; Mohammadi, A.; et al. Imparting hydrophobicity to a MOF on layered MXene for the selective, rapid, and ppb level humidity-independent detection of NH_3 at room temperature. *J. Mater. Chem. A.* **2024**, *12*, 26132-46. DOI
153. Wu, H. X.; Li, Y.; Chen, L. L.; et al. MXene-boosted nickel-based metal-organic framework composite with enhanced conductivity and catalytic activity for highly sensitive glucose detection. *Rare. Metals.* **2026**, *45*, e70442. DOI
154. Boruah, P. K.; Sharma, N.; Das, M. R.; Ohtani, R.; Le Ouay, B.; Ohba, M. Metal-organic framework/$Nb_4C_3T_x$ MXene composites for ultrasensitive detection of dopamine. *Chem. Commun.* **2024**, *60*, 7307-10. DOI PubMed
155. Shen, B.; Hong, B.; Guo, X.; et al. Facile fabrication of sensing electrode based on CoFe-MOFs/MXene for ultrasensitive detection of picomolar chloramphenicol. *Talanta* **2025**, *286*, 127552. DOI
156. Elancheziyan, M.; Manoj, D.; Bhuvanendran, N.; Harathi, J.; Lee, S. Y.; Won, K. CoFeMn-layered double hydroxide-decorated MXene for high-performance electrochemical sensing of ciprofloxacin in food and water samples. *Microchim. Acta.* **2026**, *193*, 255. DOI
157. Kaur, G.; Sharma, S.; Bhardwaj, N.; Nayak, M. K.; Deep, A. Highly sensitive and selective electrochemical detection of Aflatoxin B1 in water and Pistachio samples with MOF/MXene composite based sensor. *Food. Control.* **2024**, *165*, 110694. DOI
158. Xiao, P.; Zhu, G.; Shang, X.; et al. An Fe-MOF/MXene-based ultra-sensitive electrochemical sensor for arsenic(III) measurement. *J. Electroanal. Chem.* **2022**, *916*, 116382. DOI
159. Cheng, D.; Li, P.; Zhu, X.; Liu, M.; Zhang, Y.; Liu, Y. Enzyme-free electrochemical detection of hydrogen peroxide based on thethree-dimensional flower-like Cu-based metal organic frameworks and MXene Nanosheets. *Chin. J. Chem.* **2021**, *39*, 2181-7. DOI
160. Su, X.; You, Q.; Wang, P.; et al. MXene quantum dot functionalized bimetallic MOFs as a label-free aptasensor for highly sensitive detection of exosomes. *J. Mater. Chem. C.* **2024**, *12*, 8561-8. DOI
161. Richard, B.; Niyas, K.; Ankitha, M.; Rasheed, P. A. Biological metal-organic framework-embedded MXene nanocomposite as a wearable transducer patch for real-time monitoring of the sleep hormone. *ACS. Appl. Nano. Mater.* **2024**, *7*, 9585-97. DOI
162. Lv, L.; Kang, X.; Hua, L.; et al. Sandwich-type electrochemical immunosensor based on MXene/CNTs substrate and MOFs (MIL-101) probe for leather artifact identification. *Microchem. J.* **2025**, *213*, 113810. DOI
163. Xie, Z.; Gao, Z.; Yu, T.; Du, J.; Qiu, J. Multifunctional MXene/MOF-derived foam for adaptive radar-infrared stealth and structural sensing. *Adv. Funct. Mater.* **2025**, *36*, e30008. DOI
164. Xu, W.; Lu, Y.; Zhang, Z.; et al. MOF/MXene nanocomposite to improve thermal sensitivity and bending resistance of flexible temperature sensor for body temperature and respiration rate monitoring. *IEEE. Sensors. J.* **2024**, *24*, 9437-48. DOI
165. Wang, D.; Zhang, D.; Yang, Y.; Mi, Q.; Zhang, J.; Yu, L. Multifunctional latex/polytetrafluoroethylene-based triboelectric nanogenerator for self-powered organ-like MXene/metal-organic framework-derived CuO nanohybrid ammonia sensor. *ACS. Nano.* **2021**, *15*, 2911-9. DOI
166. Li, Y.; Liu, Y.; Wang, Z.; et al. In-situ growth of Ti_3C_2@MIL-NH_2 composite for highly enhanced photocatalytic H_2 evolution. *Chem. Eng. J.* **2021**, *411*, 128446. DOI
167. Tian, P.; He, X.; Zhao, L.; et al. Enhanced charge transfer for efficient photocatalytic H_2 evolution over UiO-66-NH_2 with annealed $Ti_3C_2T_x$ MXenes. *Int. J. Hydrogen. Energy.* **2019**, *44*, 788-800. DOI
168. Wang, Q.; Domen, K. Particulate photocatalysts for light-driven water splitting: mechanisms, challenges, and design strategies. *Chem. Rev.* **2019**, *120*, 919-85. DOI PubMed
169. Li, Z.; Fang, S.; Sun, H.; Chung, R. J.; Fang, X.; He, J. H. Solar hydrogen. *Adv. Energy. Mater.* **2023**, *13*, 2203019. DOI
170. Chen, W.; Han, B.; Xie, Y.; Liang, S.; Deng, H.; Lin, Z. Ultrathin Co-Co LDHs nanosheets assembled vertically on MXene: 3D nanoarrays for boosted visible-light-driven CO_2 reduction. *Chem. Eng. J.* **2020**, *391*, 123519. DOI
171. Qin, J.; Liu, B.; Lam, K.; Song, S.; Li, X.; Hu, X. 0D/2D MXene quantum Dot/Ni-MOF ultrathin nanosheets for enhanced N_2 photoreduction. *ACS. Sustain. Chem. Eng.* **2020**, *8*, 17791-9. DOI
172. Yu, K.; Tang, L.; Cao, X.; et al. Semiconducting metal-organic frameworks decorated with spatially separated dual cocatalysts for efficient uranium(VI) photoreduction. *Adv. Funct. Mater.* **2022**, *32*, 2200315. DOI

Disclaimer/Publisher's Note: All statements, opinions, and data contained in this publication are solely those of the individual author(s) and contributor(s) and do not necessarily reflect those of OAE and/or the editor(s). OAE and/or the editor(s) disclaim any responsibility for harm to persons or property resulting from the use of any ideas, methods, instructions, or products mentioned in the content.



© The Author(s) 2026. Open Access This article is licensed under a Creative Commons Attribution 4.0 International License (https://creativecommons.org/licenses/by/4.0/), which permits unrestricted use, sharing, adaptation, distribution and reproduction in any medium or format, for any purpose, even commercially, as long as you give appropriate credit to the original author(s) and the source, provide a link to the Creative Commons license, and indicate if changes were made.